JPL NO. 9950 - 1086

SPACECRAFT CONFIGURATION STUDY FOR THE SECOND GENERATION MOBILE SATELLITE SYSTEM

FINAL REPORT
JANUARY 1985

SUBMITTED TO:
JET PROPULSION LABORATORY
CALIFORNIA INSTITUTE OF TECHNOLOGY
PASADENA, CALIFORNIA

Contract No. 956904

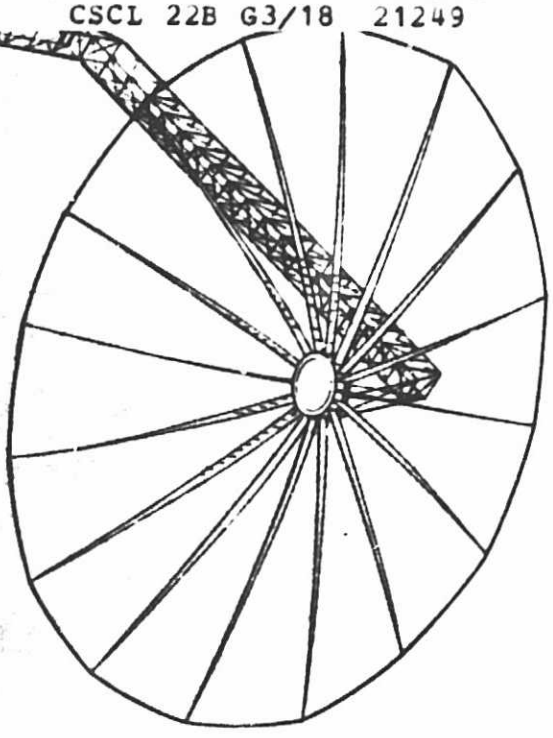

Ford Aerospace & Communications Corporation

SPACECRAFT CONFIGURATION STUDY

FOR

THE SECOND GENERATION

MOBILE SATELLITE SYSTEM

FINAL REPORT

JAN. 1985

SUBMITTED TO

JET PROPULSION LABORATORY

CALIFORNIA INSTITUTE OF TECHNOLOGY

PASADENA, CALIFORNIA

Prepared by: M. Louie
W. von Stentzsch
F. Zanella
R. Hayes
F. McGovern
R. Tyner

Ford Aerospace & Communications Corp.

3939 Fabian Way
Palo Alto, CA 94303

This report was prepared for the Jet Propulsion Laboratory, California Institute of Technology, sponsored by the National Aeronautics and Space Administration.

FORWARD

Ford Aerospace & Communications Corporation, Palo Alto, California, submits this Final Report to JPL, Pasadena, California, in fulfillment of JPL Contract Number 956904.

ACKNOWLEDGEMENT

The authors wish to express their deep gratitude to Dr. Y. H. Park and Mr. M. K. Sue of JPL, and acknowledge their fervent effort and in-depth understanding during this study.

ABSTRACT

Based upon the high power, high performance spacecraft bus being developed by Ford Aerospace & Communications Corp. (FACC), this study has investigated the Spacecraft Configuration for the second generation Mobile Satellite System (MSS) in the following areas:

1. 20 meter antenna(s) configuration;
2. Spacecraft power, dissipation, mass and physical size trade-off;
3. Needed spacecraft modifications;
4. Transponder linearization techniques.

The study results indicated that the advanced spacecraft bus being developed by FACC is capable of supporting the required payload for the second generation MSS. This study's results also point out that more attention should be given to the techniques for transponder linearization and avoidance of passive intermodulation.

TABLE OF CONTENTS

1.0 INTRODUCTION AND SUMMARY

The basis for the configuration studies for the second generation mobile satellite system (MSS) will be the Advanced Communications Satellite Bus being developed by Ford Aerospace and Communications Corporation (FACC). This spacecraft is expected to be operational and commercially available by 1990. The bus is designed to satisfy a broad range of multi-mission payload requirements in a cost effective manner. The primary objective of the bus design is the selection of a reliable approach with the lowest overall system cost. Compatibility with both STS and expendable launchers is maintained.

The bus incorporates a unified bi-propellant propulsion system capable of providing apogee injection into geosynchronous orbit for a variable beginning of life (BOL) satellite mass. The bus is 3 axis stabilized and has stationkeeping fuel and design features permitting a mission lifetime of ten years.

The satellite bus configuration is such as to provide the maximum heat rejection capability within the constraints of the booster fairing and STS envelopes. Heat pipes will be implemented in the thermal control system which is capable of maintaining the temperatures of the satellite communications equipment within a desirable range throughout the ten year life.

The satellite's solar array provides selectable (modular) power of 2000 to 3500 watts to the satellite; bus power is regulated to an operating range of 28-35V throughout sunlight and eclipse operations. Attitude control, telemetry and command processing, thermal control, and battery charging are performed in the satellite by time sharing a central processor. In addition,

the central processor provides the control functions for the propulsion stage required for launches from the STS for perigee injection. The perigee propulsion stage functions are integrated with those of the satellite through perigee injection and its ultimate separation from the satellite.

The satellite bus configuration is such that modular construction allows substitution of communications modules and antennas for differing payload requirements from program to program.

Non-communications payload bus hardware is standardized to provide the broadest range of applicability to future projected commercial satellite program. Determining the design features of the FACC Advanced Satellite Bus for the MSS program is the principal objective of this study. The study is performed to synthesize the design of the satellite to accommodate the payload(s) as defined by JPL.

In the study, it was found that there are several dominant factors which constrains the design of the MSS spacecraft. They are:

- o the physical size of the antenna package (including reflector and deployment boom);
- o the mass of the antenna(s) system;
- o The RF/DC efficiency of the UHF high power amplifier (HPA).

The required dissipation of the spacecraft is less serious than other constraints.

Based upon characteristics of the Advanced Communications Satellite Bus being developed by FACC, several trade-off studies have been performed to

optimize the spacecraft configuration for its mass, power and physical size. These preliminary studies have the following results:

1. A single 20 meter antenna can be packaged into the existing spacecraft bus. A two-antenna configuration requires some modification of the existing spacecraft bus and a new perigee stage.

2. With a single antenna configuration, for both transmit and receive, passive intermodulation (PIM) might become a problem and cause unacceptable system degradation. To avoid or minimize the passive intermodulation interference, special guidelines should be implemented in the frequency allocation and design of the communications system.

3. The existing power subsystem can provide sufficient DC power for the second generation MSS satellite if the HPA/linearizer can achieve a RF/DC efficiency of 30%. If the linearization techniques cannot be implemented or are too complicated to incorporate into the spacecraft, then the available RF power would be reduced.

4. Initial analysis indicated that the existing attitude control system can handle the solar pressure effects caused by the large size reflector and the deployment boom. The analysis also indicated that the existing spacecraft, with a single antenna configuration, can achieve the required pointing accuracy.

2.0 The Second Generation Mobile Satellite System Requirement and Study Considerations

2.1 Basic System Description

The second generation land mobile satellite is designed to be operative during the year 1992 using 1990 technology. It is designed to provide voice and data communication to mobile users throughout a vast geographic area: CONUS, Alaska and Canada. Utilizing multiple spot beams, a high power spacecraft bus, and frequency re-use, the usual power and bandwidth constraints could be somewhat alleviated and thousands of channels could be providing service to hundreds of thousands of users. The system, as currently conceived by JPL, consists of a space segment and a ground segment. In this study, we concentrate on the space segment.

The baseline space segment consists of two satellites - one at 90°W and the other at 130°W. Only the east satellite is considered for the purpose of the spacecraft configuration study.

The satellites are assumed to be operating at the UHF and Ku-Bands. The UHF frequency is for links between the satellite and mobile terminals. The Ku-Band is for links between satellite and the gateway station or Network Management Center. Tables 2-1 and 2-2 summarize the baseline design, its requirements, and assumptions provided by JPL. The baseline design also assumes a non-overlapping feed design, i.e., one feed element per beam. A simplified block diagrams of the communications payload is provided in Figure 2-1.

To achieve 2 to 4 times frequency reuse for each satellite, the 10 MHz UHF band is divided into 7 frequency sub-bands, approximately 1.4 MHz each. Each of the multiple UHF beams is assigned to operate in one of the seven sub-bands with some frequency sub-bands being reused 2 to 4 times. Figure 2-2 shows the footprints of the east satellite and its frequency reuse plan.

2.2 Required Satellite RF Power, Antenna Pointing Accuracy and Antenna Characteristics

To meet the system requirement, a spacecraft bus which can provide an average RF power of 300 watts to 500 watts has been selected. The required RF power will normally be distributed equally to the 24 beams. Due to the different traffic intensity in each beam coverage area, the instantaneous power per beam may be substantially higher or lower than the average power. The selected spacecraft should be designed to handle this power variation.

To achieve maximum frequency reuse, a 20 meter UHF antenna is chosen for the system. With this 20 meter reflector, the crossover beamwidth for each beam is about 1.4 degrees. The required pointing accuracy and stability is 0.15 degrees to minimize antenna pointing loss and interference.

The Ku-Band antenna is about 0.4 meters in diameter and requires a pointing accuracy of about 0.2 degrees.

TABLE 2-1

Second Generation Mobile Satellite System Assumptions and/or Requirements (Baseline Design)

Operating Time Frame	1992-2000
Technology	1990
Satellite Bus	Next Generation High Power Satellite Buses
No. of Satellites	2
Satellite Locations	
East Satellite	90° W
West Satellite	130° W
Operating Frequency	
UHF (uplink)	821-825, 845-851 MHz
(downlink)	866-870, 890-896 MHz
Ku-Band (uplink)	13.2 GHz
(downlink)	11.65 GHz
Assumed Bandwidth	
UHF	10 MHz (4 MHz & 6 MHz)
Ku-Band	50 MHz
Number of Multiple Beams	
UHF	21 (West Sat) 24 (East Sat)
Ku-Band	1
Antenna Size	
UHF	20 meters
Ku-Band	0.4 meters
Required Satellite RF Power	
UHF	300 W (min), 500 W (max)
Ku-Band	10 W

TABLE 2-2

Additional Baseline Assumptions and/or Requirements

System Parameters

Number of Satellites	2
Satellite Locations	90° W and 130° W
Frequency, MHz (uplink)	821-825, 845-851
(downlink)	866-870, 890-896
UHF Bandwidth, MHz	10
Channel Spacing, KHz	5
Backhaul Frequency, GHz (uplink)	13.2
(downlink)	11.65
Backhaul Bandwidth, MHz	50
No. of Backhaul Beams	1

Satellite Parameters

System Noise Temperature, dB-K	29
Carrier-to-Intermod Ratio, dB	24-26
Pointing Accuracy, degrees	0.15
Required EIRP, dBw/channel	
UHF	28.69
Ku	4.3
Required Satellite RF Power, Watts	
UHF	300 (min), 500 (max)
Ku	10

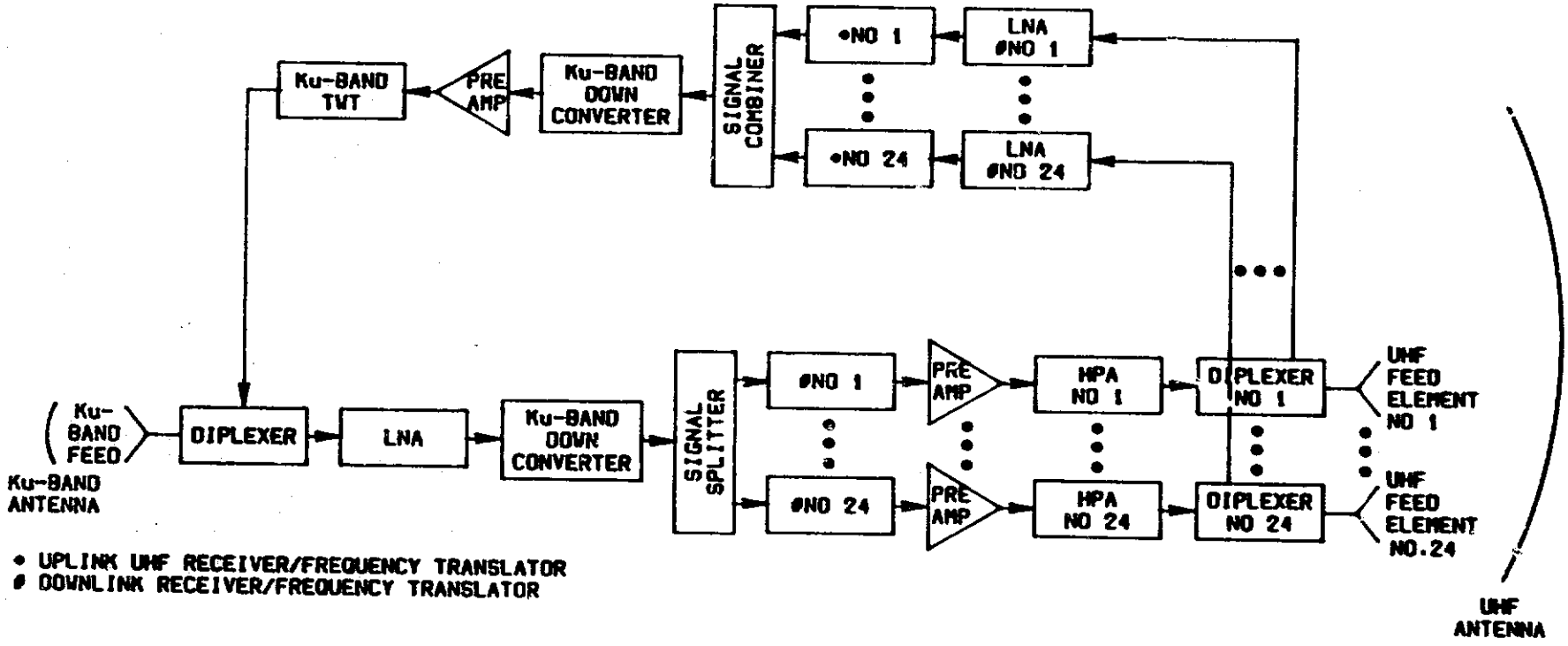

FIGURE 2.1
SIMPLIFIED BLOCK DIAGRAM OF THE COMMUNICATIONS PAYLOAD

FIGURE 2-2. LMSS SATELLITE ANTENNA BEAM LAYOUT

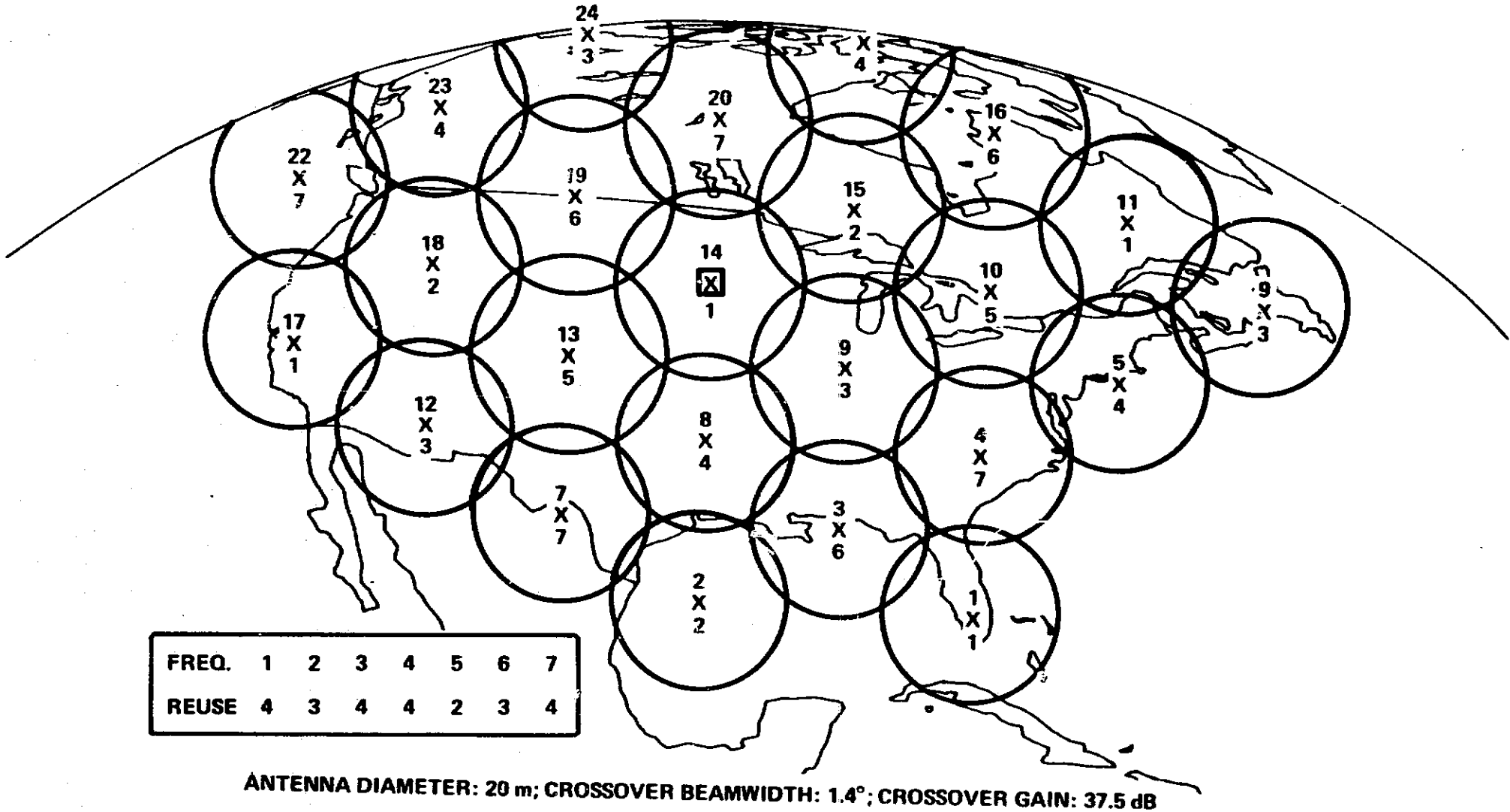

ANTENNA DIAMETER: 20 m; CROSSOVER BEAMWIDTH: 1.4°; CROSSOVER GAIN: 37.5 dB

SATELLITE POSITION: 90° W LONGITUDE GEOSTATIONARY ORBIT

2.3 Study Objectives and Considerations

The objective of this study is to provide JPL with a spacecraft configuration design for the second generation land mobile satellite. In our study, the spacecraft selected is the high power, high performance spacecraft being developed by Ford Aerospace and expected to become commercially available in the early 1990's. The study includes the following tasks:

1. Spacecraft and antenna configuration study;

2. Spacecraft DC Power, Power Dissipation and Mass

3. Specific Modifications Needed for the MSS

4. Antenna Feed Study.

In addition, a survey of linearization techniques for the UHF and L-Band spaceborne power amplifiers will also be conducted.

To understand the problem and define it into some workable areas, we selected a study methodology which is illustrated in Figure 2-3. In this study, our efforts have been divided into two major areas:

1. MSS payload and its power, mass and dissipation requirements;

2. Spacecraft bus and how to package the required payload onto the spacecraft bus under development.

In the first task, the selection and packaging of the 20 meter reflector(s) becomes a major issue. A single antenna for both transmit and receive utilize the space mass efficiently. However, a common antenna for

FIGURE 2-3. LMSS CONFIGURATION TRADES

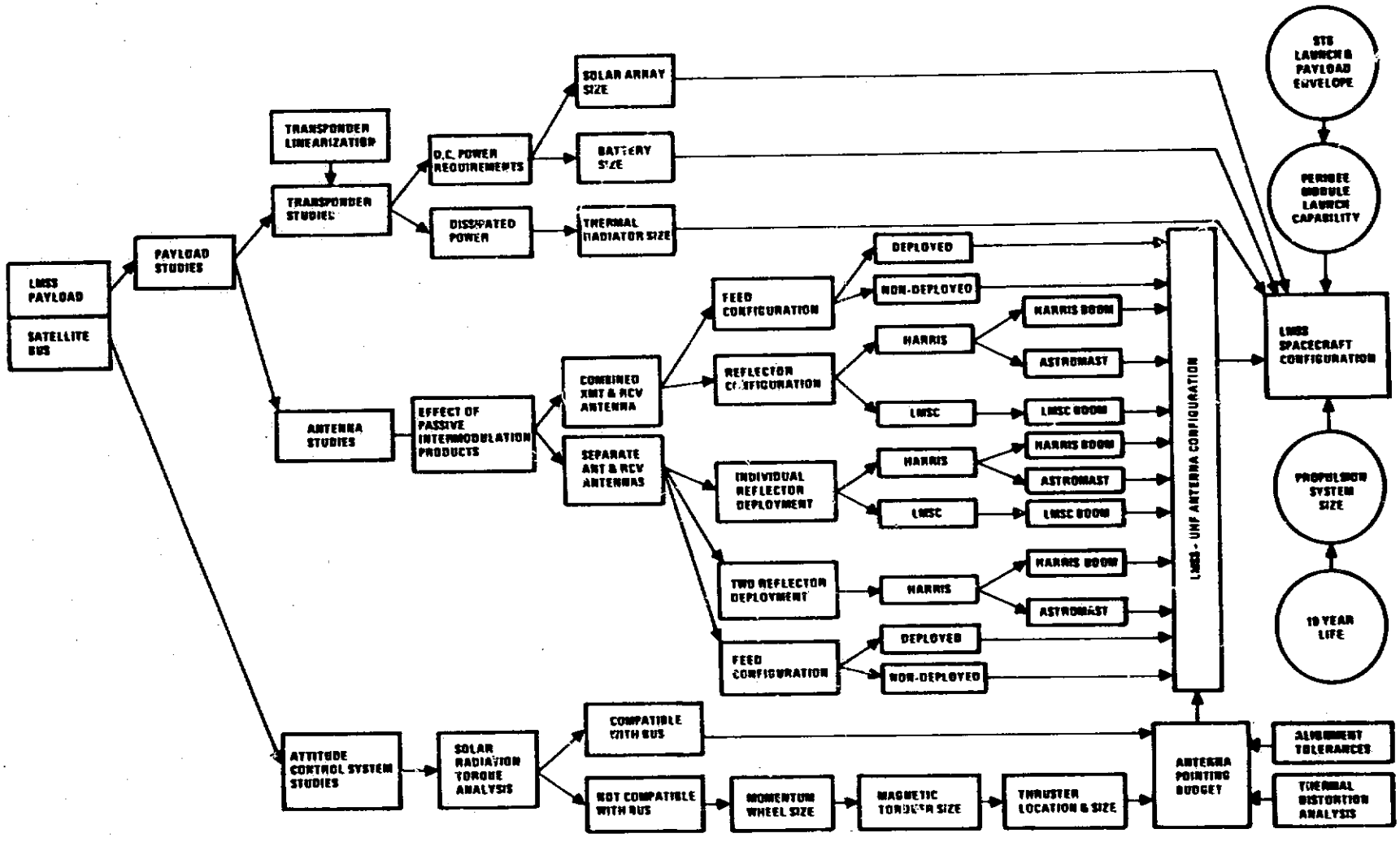

Ford Aerospace & Communications Corporation

both transmit and receive may have potential problems in passive intermodulation. This trade-off study of several antenna configurations was performed in the study. Several candidate antenna systems are also evaluated. In the selection of the reflector(s), weight and size of the reflector are the critical criteria in the selection process, because the selected payload should be implemented for STS launch with an existing (or developing) spacecraft. The weight and physical constraints play an important role in packaging the desired payload into the existing bus without violating the STS launch envelope and the existing bus launch weight.

As in most spacecraft designs, DC power capability is another constraint. Initially, the requirement of 500 watts (maximum) RF power and 50% eclipse capability does not seem to be a problem. However, further investigation revealed that the efficiency of the high power amplifier (HPA) is a determining factor in deciding whether the required payload can be fitted into the FACC bus. If the RF/DC efficiency of the HPA is only 20% then the required solar array power requirement will be 3364 watts and the thermal dissipation in the communications module is 2400 watts. This change will result in a dry spacecraft mass increase of 16.9 kg for the solar array and 18.6 kg for the thermal and structural subsystems. Careful judgment must be given to implement this change since the dry spacecraft mass margin, of a maximum mission perigee module, will be reduced by 36%. Physical changes to the FACC bus can be readily accommodated since ample margin exists between it and the limiting STS payload envelopes. With this consideration, the linearization of the HPA becomes an important factor in the spacecraft configuration study.

In a multiple-carrier operation, most of the high power amplifiers (HPAs) have to be operated in a "back-off" mode to minimize the effects of intermodulation. In general, DC/RF conversion efficiency decreases with the amount of backoff. From a spacecraft standpoint, the backoff required to achieve 22-24 dB C/IM value may result in unacceptably low DC/RF efficiency. Should this occur, linearization techniques, which "make" the HPA more linear thus reduce intermodulation levels, would become another important factor in sizing the spacecraft power subsystem. To assess the impact of linearization on the spacecraft configuration, several linearization techniques were investigated in the study. However, each linearization technique has its advantages and disadvantages. Some techniques require complex circuitry and some techniques require additional amplifiers. All of them introduce new hardware, thus increasing the weight of the communications payload. To select an optimum and practical linearization technique, a detailed trade-off among complexity, power and mass has to be conducted. Due to the limited scope of this study, only a general survey and a preliminary evaluation can be performed for the linearization techniques.

Considering all these factors, the spacecraft configuration study appears to become a classical spacecraft trade-off study among mass, power, dissipation and physical size.

3.0 MSS SPACECRAFT CONFIGURATION

Our choice for the 2nd generation MSS spacecraft configuration is represented by a single UHF antenna system, using the Lockheed Missiles and Space Corp. (LMSC) wrap-rip reflector and deployment boom. This conclusion was reached based on the antenna configuration tradeoff outlined in Section 3.1 as well as the following criteria:

- o MSS system requirements
- o Available STS payload envelope
- o FACC spacecraft bus compatibility
- o FACC perigee stage launch mass capability

FIGURE 3-1. LMSS ON ORBIT CONFIGURATION

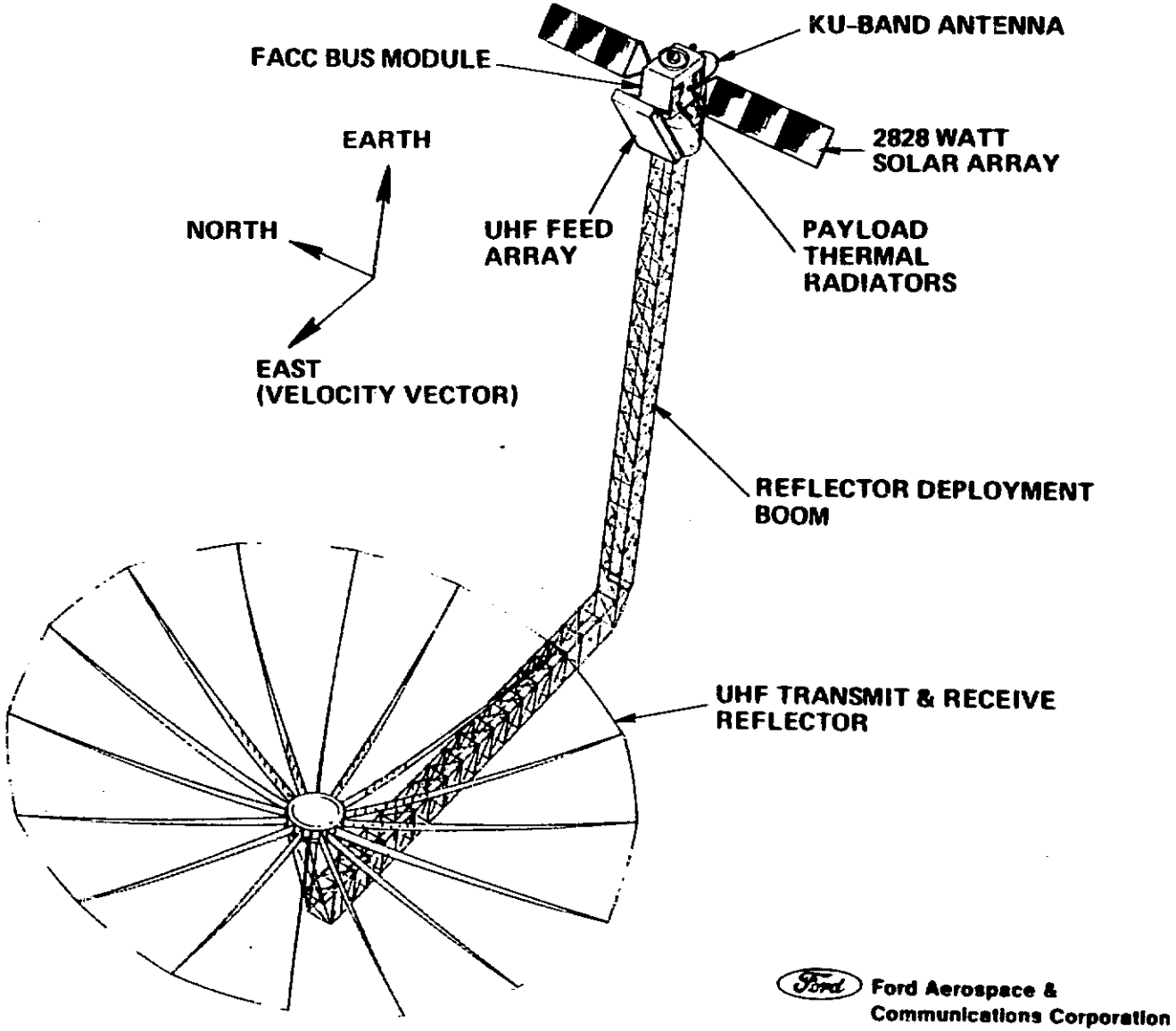

Figure 3-1 shows an on-orbit perspective sketch of the baseline FACC/MSS spacecraft configuration. The most striking feature is the unfurled 20.0 meter diameter UHF/LMSC wrap-rip reflector on the east side of the satellite. The reflector is deployed with its deployment boom in the anti-earth direction. To minimize the impact on the attitude control system a minimum structural frequency of 2 Hz is desirable for the reflector and boom. The RF beam is pointed northward to look at the contiguous U.S., Alaska and Canada. The reflector is illuminated by either a 21 or 24 element feed located on top of the FACC spacecraft bus communications module. This location will keep the RF transmission line losses from the feed to the transponder at a minimum. The FACC spacecraft bus is in principle a rectangular box which measures 2.6 meters long by 1.7 meters high by 1.6 meters wide. The box is located such that the widest dimension is oriented to look in the north and south directions to assure maximum thermal radiator area available for the payload equipment. The MSS transponder is located on the inside of this box on the north and south panels. Each honeycomb panel has heatpipes sandwiched in between them and Optical Solar Reflectors (OSR) on the outside to distribute the thermal heat load and control the temperature of the equipment. Areas of the satellite that do not have high thermal power dissipations are covered externally by multi-layer insulating blankets.

In contrast to the large UHF antenna the Ku-Band antenna is only 0.4 meters in diameter. It is an offset-feed design and is located on the west side of the spacecraft bus.

The FACC/MSS spacecraft is a modular design to simplify its assembly, integration and testing. These modules can be described as follows:

a. Spacecraft Support Cradle provides the electrical and mechanical interface between the satellite and the STS.

b. Perigee Stage Module provides the impulse to inject the vehicle from the STS parking orbit into the geosynchronous transfer orbit. It also provides the mechanical and electrical interface between the support cradle and the MSS spacecraft.

c. Spacecraft Bus consists of two modules. They include the Communications Module which houses the communications transponder equipment located on the north and south panel radiators for maximum thermal power dissipation capability. A Subsystems Module supports the housekeeping functions of the spacecraft. Among them is the bipropellant propulsion system which provides the impulse and control at apogee to change from geosynchronous transfer orbit to geosynchronous orbit as well as stationkeeping maneuvers for ten years. Also included is the Attitude and Orbit Control System (AOCS) hardware including momentum wheels, rate gyros, earth and sun sensors and their associated electronics equipment. The power control system supplies and controls the DC power requirements of the payload and housekeeping equipment. Major components of this system are batteries, power control unit, shunt and the solar array. The solar array also is modular since additional panels may be added to satisfy the specific power requirements of the payload. The subsystem module also supports the Telemetry, Tracking and Command equipment.

d. The Antenna Module contains the feed assembly, as well as the reflector and boom assemblies.

If the passive intermodulation products of the combined transmit and receive antennas present a problem then an alternate solution should be considered. The solution can be to have two separate antennas, one for transmit and one for receive, which are deployed individually. There are two basic problems associated with this concept. One, the envelope of the LMSC reflectors and booms stowed side by side exceeds the STS payload envelope and second, the launch mass capability of the FACC stage is exceeded. The first problem may be solved by reducing the 20.0 meter antenna aperture a small amount to reduce the the stowed envelope of the reflector and boom. The second problem is that the fully fueled spacecraft exceeds the capability of the FACC perigee stage by 558 kg. This can be remedied by using a new perigee stage based on the SRM-1 solid propellant motor manufactured by the Chemical Systems Division of United Technologies Laboratory (CSD/UTC).

3.1 Antenna Configuration Tradeoff

To meet the MSS mission requirements, five antenna configurations were considered for this study. Table 3-1 summarizes the results of this tradeoff which includes the following UHF antenna system possibilities:

A1 Two LMSC reflectors deployed individually from a FACC bus.

A2 Two Harris reflectors deployed together from a FACC bus.

B1 A single LMSC reflector deployed from a FACC bus.

PARAMETER \ CONFIGURATION	A1	A2	B1	B2	B3
	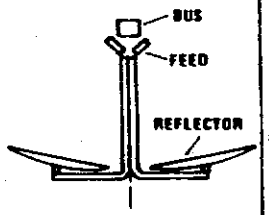	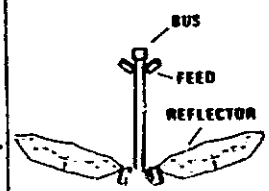	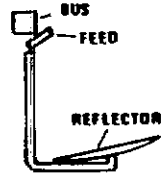	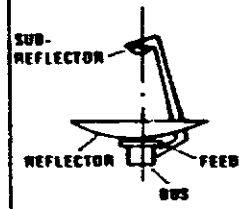	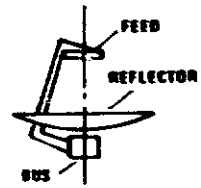
• ANTENNA CONFIGURATION	DUAL UHF; OFFSET FED DUAL DEPLOYMENT; LMSC	DUAL UHF; OFFSET FED SINGLE DEPLOYMENT; HARRIS	SINGLE UHF, OFFSET FED, LMSC	SINGLE UHF, CASSEGRAIN	SINGLE UHF; CENTER FED
• ADVANTAGES	• NO PASSIVE INTERMODS • CLEAR ANTENNA FOV • SHORT RF PATH FROM FEED TO TRANSPONDER • SYMMETRIC CONFIGURATION MINIMIZES SOLAR TORQUE IMBALANCE	• NO PASSIVE INTERMODS • CLEAR ANTENNA FOV • SHORT RF PATH FROM FEED TO TRANSPONDER • CAN BE STOWED IN STS ENVELOPE • SYMMETRIC CONFIGURATION MINIMIZES SOLAR TORQUE IMBALANCE	• CLEAR ANTENNA FOV • SHORT RF PATH FROM FEED TO TRANSPONDER • CAN BE STOWED IN STS ENVELOPE • CAN BE LAUNCHED WITH FACC PERIGEE STAGE	• SHORT RF PATH FROM FEED TO TRANSPONDER • CAN BE STOWED IN STS ENVELOPE	• CAN BE STOWED IN STS ENVELOPE
• DISADVANTAGES	• STOWED REFLECTORS & BOOMS EXCEED STS ENVELOPE • LONG REFLECTOR DEPLOYMENT MAXIMIZES THERMAL DISTORTION • S/C TOO HEAVY FOR FACC PERIGEE STAGE	• LONG REFLECTOR DEPLOYMENT MAXIMIZES THERMAL DISTORTION • S/C TOO HEAVY FOR FACC PERIGEE STAGE	• PASSIVE INTERMODS • LONG REFLECTOR DEPLOYMENT MAXIMIZES THERMAL DISTORTION	• PASSIVE INTERMODS • FOV BLOCKAGE • COMPLEX SUB-REFLECTOR DEPLOYMENT	• PASSIVE INTERMODS • FOV BLOCKAGE • LONG RF PATH FROM FEED TO TRANSPONDER • COMPLEX FEED DEPLOYMENT

TABLE 3-1. LMSS – ANTENNA CONFIGURATION TRADEOFF

B2 A single center-feed Cassegrain antenna system.

B3 A single center-fed prime focus antenna system

As the following paragraphs will demonstrate configuration B1 is the best choice based on STS envelope restrictions and the FACC perigee stage launch mass capability. A mass comparison between the LMSC and Harris Corp. reflector and deployment systems can be found in Table 4.3-3.

3.1.1 Antenna Configuration A1 - Dual LMSC Antenna Reflectors

This configuration is the best choice from the antenna design standpoint. No passive intermodulation products are created because the transmit and receive antennas are separated. In this concept each 20 meter diameter LMSC reflector is deployed individually away from the FACC bus using the LMSC deployment boom. Unfortunately there are two basic problems with this approach. One is that in a horizontal STS launch configuration the stowed envelopes of the LMSC reflectors and booms exceed the STS payload envelope. Since this interference is small, optimization of the reflector and boom diameter might allow stowage within the STS payload envelope. The second problem is that the dry launch mass of 1491 kg exceeds the capability of 1247 kg of the FACC perigee stage vehicle. Alternate perigee stages such as the one using the CSD/UTC SRM-1 perigee motor can be considered to launch a spacecraft with this configuration.

3.1.2 Antenna Configuration A2 - Dual Harris reflectors

The antenna design benefits of this configuration are identical to that of A1. The idea behind this concept was to deploy the Harris Corp.

Deployable Truss Structure (DTS) reflectors with a single deployment boom. After deployment of the stowed reflectors they are allowed to unfold from their respective edges. The stowed 20 meter diameter reflectors and the deployable boom can be stowed within the STS payload envelope. In principle this concept is sound, however the mass of the reflectors and boom, 181 kg each and 454 kg respectively, required modification of the existing spacecraft bus and a new perigee stage to deliver the spacecraft to the geosynchronous orbit.

3.1.3 Antenna Configuration B1 - Single LMSC Reflector

The principle of this concept is to deploy a single LMSC reflector away from the spacecraft bus using an LMSC deployment boom. The advantage of this approach is that the stowed reflector and boom can be readily placed in the STS payload bay envelope. Also the dry spacecraft launch mass of 1218 kg can be accommodated by the FACC perigee stage vehicle. For the above reasons this configuration is the best choice for the MSS spacecraft. Since transmit and receive antennas are combined, passive intermodulation products are a concern for this configuration.

3.1.4 Antenna Configuration B2 - Center-fed Cassegrain Antenna

The thought behind this concept was to explore possible benefits of a center-fed cassegrain antenna geometry. In this configuration the LMSC main reflector would be placed on top of the spacecraft bus and a subreflector would be deployed away to its proper geometric position. The feed also would be placed on top of the bus to minimize the RF path losses to the transponder. The stowed spacecraft can fit inside the STS payload envelope. The biggest

problem with this configuration is that the field of view of this antenna is blocked by the large subreflector and its deployment structure. In addition the mechanism for such a structure will be very complex. Since transmit and receive antennas are combined passive intermodulation products are a concern for this configuration.

3.1.5 Antenna Configuration B3 - Center Fed Antenna

This center-fed antenna geometry was also considered but after short examination it became obvious that too many problems make this configuration impractical. The 2.0 X 4.0 meter feed and its deployment structure cause too much blockage of the RF beam. Also the RF transmission line losses from the feed to the transponder are large. In addition the mechanism required to deploy the feed will be very complex. Since transmit and receive antennas are combined the passive intermodulation products are of concern for this configuration.

3.2 Single Antenna Spacecraft Configuration

This spacecraft configuration was chosen as the prime candidate for the MSS mission. It is based on a single 20 meter diameter LMSC wrap-rib reflector and the LMSC deployment boom. This concept is compatible with the STS payload envelope and this spacecraft can be launched by the FACC perigee stage vehicle.

3.2.1 Deployed Spacecraft Configuration

An on-orbit picture of the MSS spacecraft can be seen in Figure 3-2. The most striking feature is the 20.0 meter diameter unfurlable UHF antenna reflector that is deployed 24.5 meters away, towards the east, from the FACC spacecraft bus using the deployable boom. The reflector is deployed to provide an F/D ratio of one and also to have a sufficient offset to provide a clear field of view for the RF beam looking towards the earth. The UHF feed is rotated into position to illuminate the reflector. The feed is closely coupled to the payload module minimizing the RF line losses. The 2828 watt solar array consists of two wings each having three panels which are extended towards north and south respectively. The wingspan of this array is 18.0 meters. The antenna reflector for this configuration is a LMSC wrap-rib design that has 20 radial ribs that are covered with a gold plated molybdenum mesh. The 20 ribs will provide a surface accuracy of the parabolic reflecting surface of LAMBDA/60. The choice of the reflector deployment boom is also the LMSC design since it and the reflector have the least mass.

FIGURE 3-2. LMSS - DEPLOYED CONFIGURATION - LMSC ANTENNA

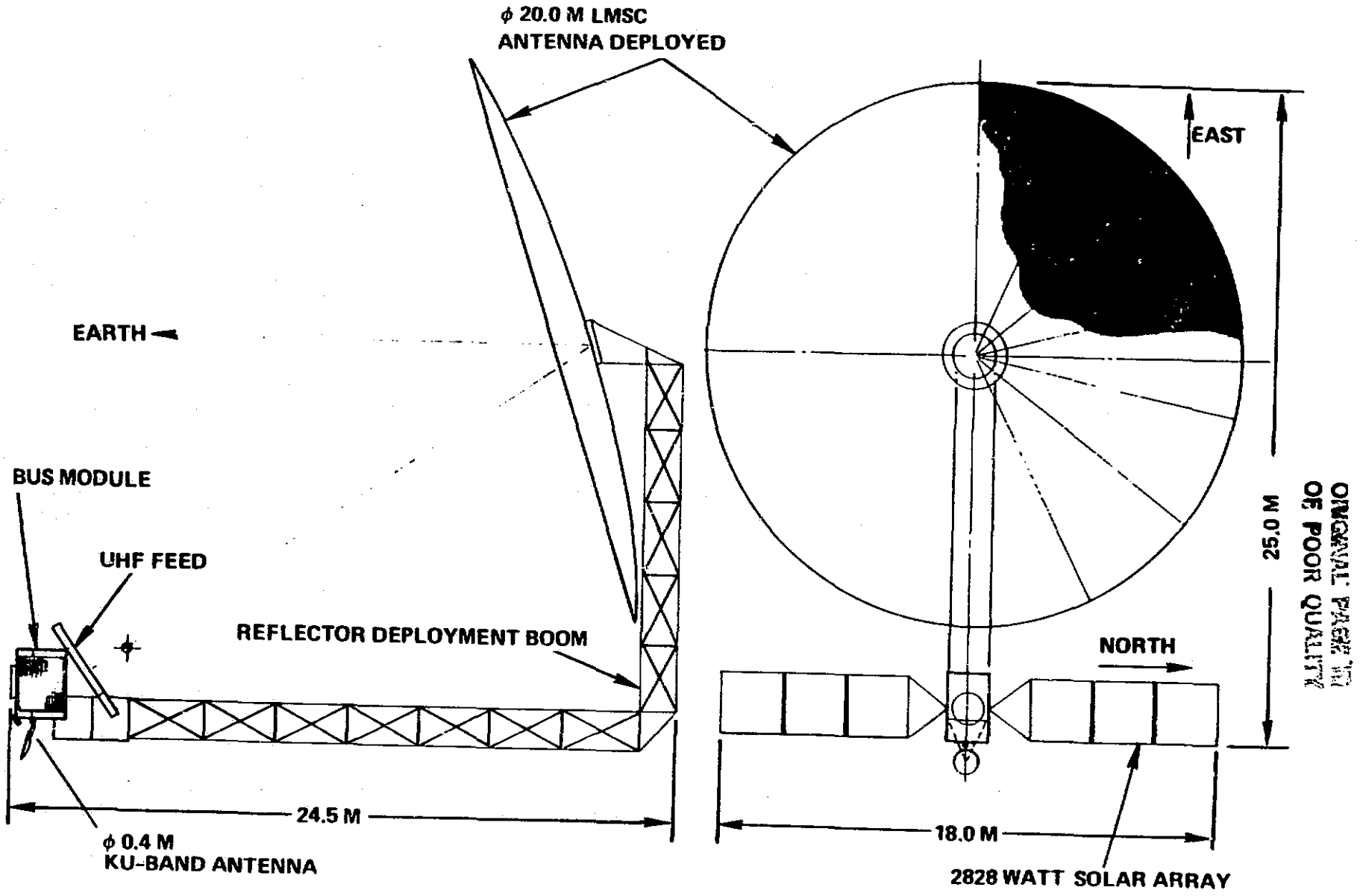

3.2.2 Stowed Spacecraft Configuration

Figure 3-3 is an illustration of what the MSS spacecraft might look like when it is stowed in the STS payload bay. The size of the stowed LMSC reflector and boom dictates that the spacecraft is launched in the horizontal position. To facilitate assembly, integration and testing the satellite is divided into independent modules: the spacecraft support cradle, perigee stage module, subsystems bus, module, payload bus module as well as the antenna module. The total length of this assembly in the STS bay is 7.2 meters. As can be seen in the picture the 2.8 meter diameter, 3.0 meter long, stowed LMSC reflector and boom assembly control the configuration of this layout. The antenna module is mounted directly on top of the FACC bus module central cylinder to provide the most direct structural load path through the perigee stage cradle into the STS keel and longeron fittings. The large size of the feed requires it to be stowed for launch adjacent to a support structure. A simple 57 degree rotation about the hinge axis will place it in the proper position to illuminate the reflector. The deployed feed is located as close as possible to the payload transponder to minimize the RF line losses.

Concepts having a fixed UHF feed were investigated but the sheer size of 2.0 X 4.3 meters of a 21 beam feed array make this solution impractical.

The 2828 watt solar array is divided into two solar array wings. The wings, consisting of three panels covered with solar cells and a deployment yoke, are stored adjacent to the north and south side of the satellite module respectively. Ample room is provided to enlarge the solar panels or to add panels if the DC power requirement if the MSS transponder should grow.

FIGURE 3-3. LMSS STOWED CONFIGURATION SINGLE LMSC ANTENNA

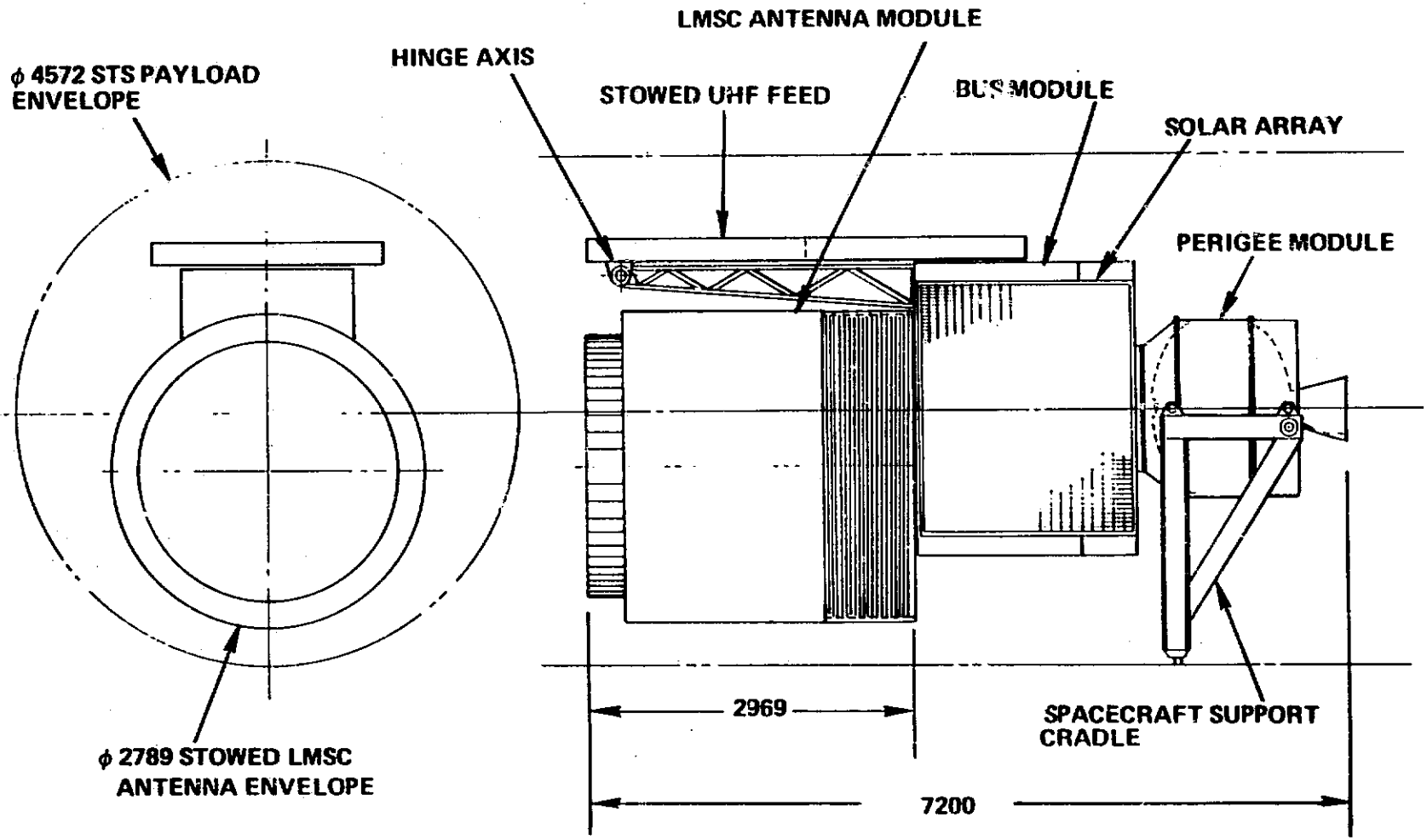

The perigee stage module provides the necessary impulse to propel the spacecraft into the geosynchronous transfer orbit from the STS parking orbit. Since the propulsion motor is of the solid propellant type the spacecraft will have to be dynamically balanced. Along with this motor the module contains the necessary adapters and spacecraft separation systems. The spacecraft support cradle provides the mechanical and electrical interface between the satellite and the STS orbiter.

3.3 Dual Antenna Spacecraft Configuration

Since two independent transmit and receive UHF antenna systems is the best solution to minimize the passive intermodulation products, therefore making the electrical design much simpler, this concept was studied in some detail. The following paragraphs and illustrations of this section describe Harris Corp. reflectors and deployment boom. LMSC reflectors and booms were considered but not shown in detail since the stowed envelope of two wrap-rip reflectors and their deployment boom exceed the STS envelope. Subsequent optimization of this boom diameter to obtain a minimum structural of the deployed system frequency of above 2 Hz or optimization of the reflector diameter might make it possible to stow two reflectors.

3.3.1 On-Orbit Spacecraft Configuration

The on-orbit configuration shown in Figure 3-4 was developed to evaluate the effect of adding a second UHF antenna system to the spacecraft. For this concept two Harris Corp. Deployable Truss Structure (DTS) reflectors and a single deployment boom were studied. These systems were considered since their stowed volumes can fit inside the STS payload envelope. The two stowed reflectors are deployed 25.7 meters in the anti-earth direction. After their deployment the DTS reflectors, which in this case are mounted on their respective edges, are allowed to unfold in the east or west direction. The span across these reflectors measures 48.0 meters. The spacecraft 2828 watt solar array wings are deployed in the north and south direction with a wingspan of 18.0 meters. Again in this configuration the two UHF feeds are closely coupled to the communications transponder. Even though the principle of the dual antenna configuration is sound the mass of 181.0 kg for each reflector and 454.0 kg for the deployment structure make this an impractical solution.

FIGURE 3-4. LMSS - DEPLOYED CONFIGURATION - HARRIS ANTENNAS

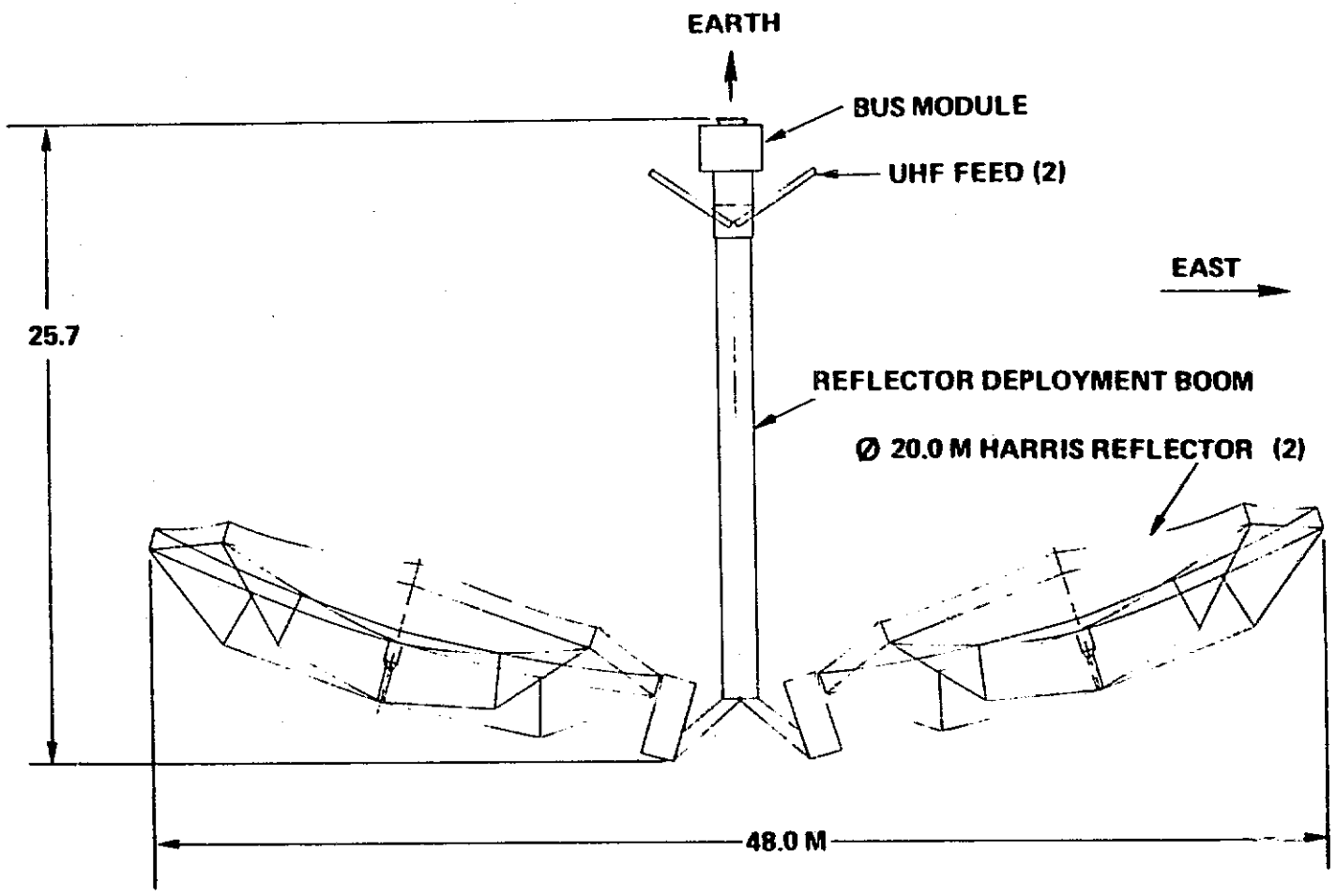

3.3.2 Stowed Spacecraft Configuration

A stowed configuration of this antenna concept can be seen in Figure 3-5. The stowed envelope dimensions of the HARRIS Corp. reflectors and boom require the spacecraft to be placed horizontally in the STS payload bay. In this position it will occupy 7.2 meters in length of the available 28.3 meters. The cross-sectional view of the STS payload envelope shows that two 2.0 meter diameter stowed reflectors can be readily accommodated in the 4.6 meter diameter envelope. The two UHF feeds measuring 2.0 X 4.0 meters need to be stowed for launch. A simple rotation of 57° about a hinge axis is required for each feed to lock in its proper on-orbit position. The feeds are located as close as possible to the communication transponder located in the FACC payload module. The rest of FACC spacecraft bus, including solar arrays, perigee stage module and the spacecraft support cradle is identical to one described in Section 3.2.2.

3.4 Harris Reflector System

The following paragraphs provide a short description of an unfurlable reflector system manufactured by Harris Corporation, Government Aerospace Systems Division in Melbourne, Florida.

3.4.1 Harris Antenna Reflector Design Concept

The Deployable Truss Structure (DTS) design represents an extension of the proven Harris radial rib technology. The DTS design evolves from the existing radial rib technology in two steps. First, a truss structure is

FIGURE 3-5. LMSS STOWED CONFIGURATION - DUAL HARRIS ANTENNA

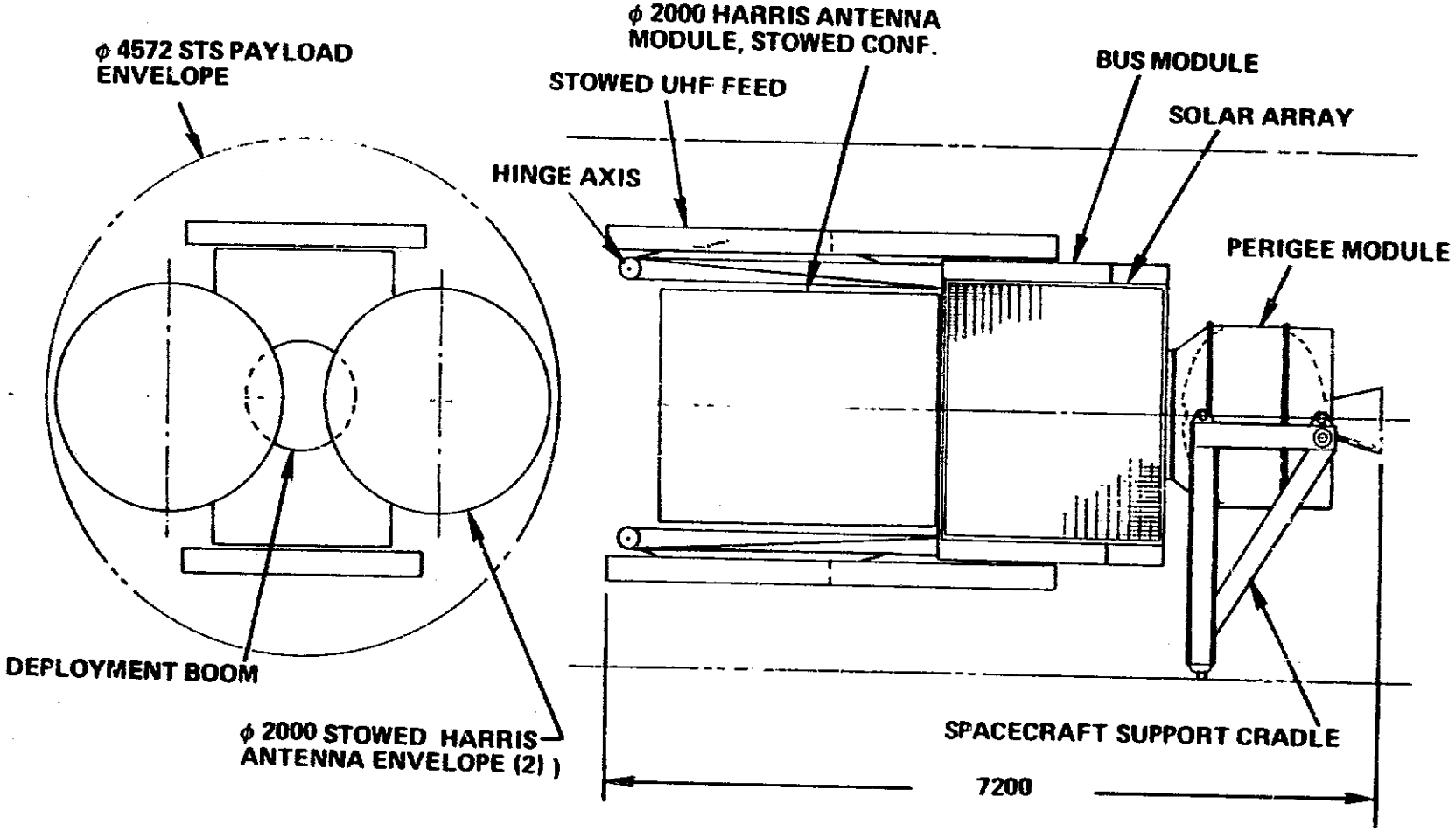

added to the rib in order to provide increased stiffness. Next the rib is segmented and the segments connected via articulating joints in order to provide a more compact stowed package. Since the rib shape is not extremely critical to the contour accuracy in our design, the rib segments are made from straight graphite tubes. Figure 3.4-1 shows a typical section of a reflector geometry which includes elements of the truss rib as well as the members which connect adjacent ribs.

Figure 3.4-2 illustrates a single partially deployed rib. Latching joints are shown at two locations, inboard and outboard of the intersection of the radial rib members and the compressive, vertical strut. These latching joints must lock to form inboard and outboard rigid members. The nonlatching joint between them must remain free to rotate in the plane of the truss preserving the structural characteristics of the pin-jointed truss. Small clips, or rod guides, attached to the main structural members and joints, support the tension rods while stowed. The deployment of the rib pulls the rods free from the rod guides. A four-bar linkage connecting the radial rib members synchronizes and controls the deployment.

3.4.2 Stowed Reflector Concept

A typical stowed DTS reflector can be seen in Figure 3.4-3. The stowed envelope of a 20.0 meter diameter reflector aperture is 2.0 meters in diameter by 2.5 meters long. To clarify this picture the reflector mesh and surface cords have been omitted. The stowed reflector is unfolded using a Mechanical Drive System (MDS) which controls the deployment of the reflector. It is located at the upper end of the hub and is attached to the innermost radial-rib member. Deployment force is transmitted to the other three radial

FIGURE 3.4-1. DTS - TWO-RIB GEOMETRY AND MATERIALS

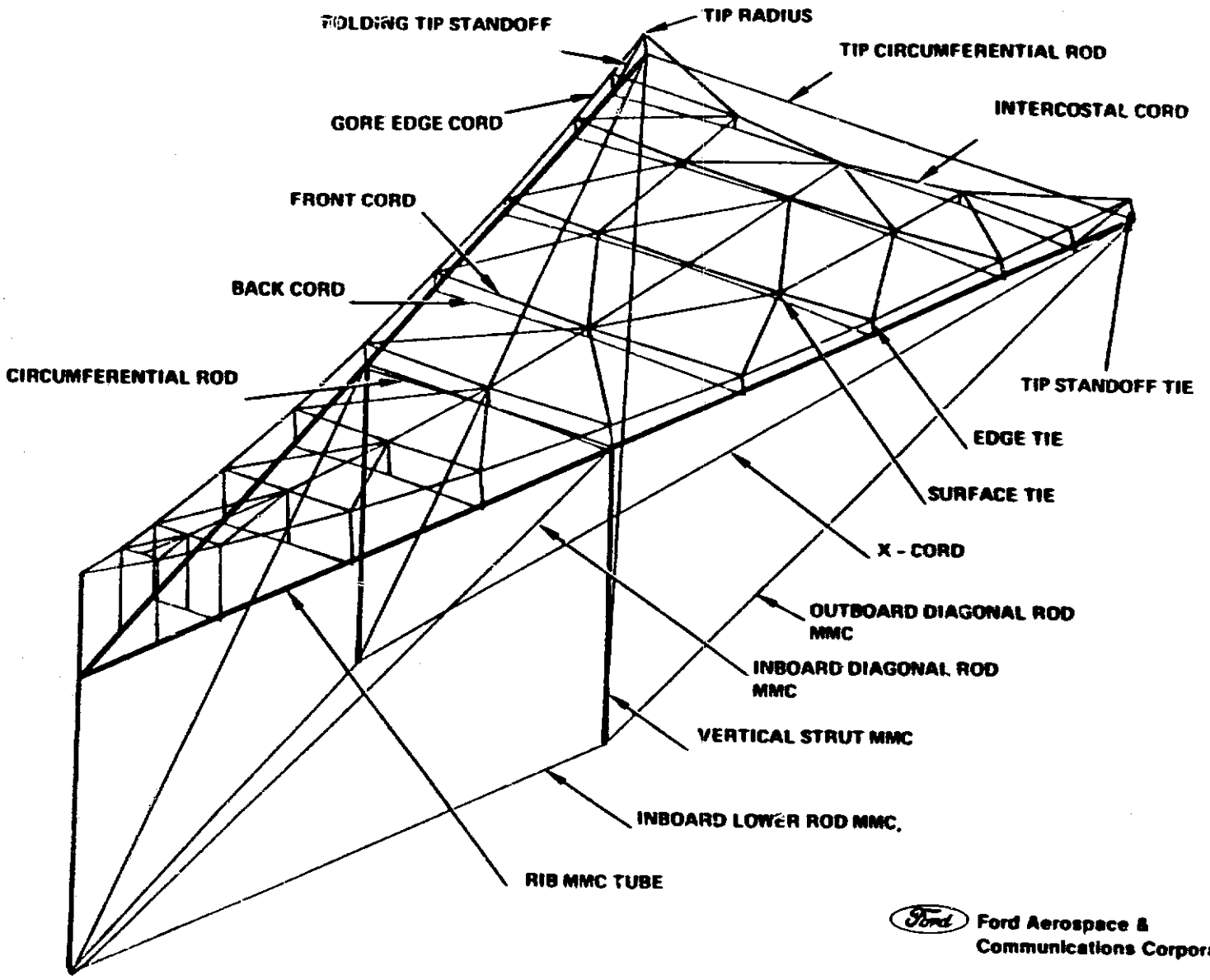

FIGURE 3.4-2. RIB DEPLOYMENT SEQUENCE – INTERMEDIATE PHASE

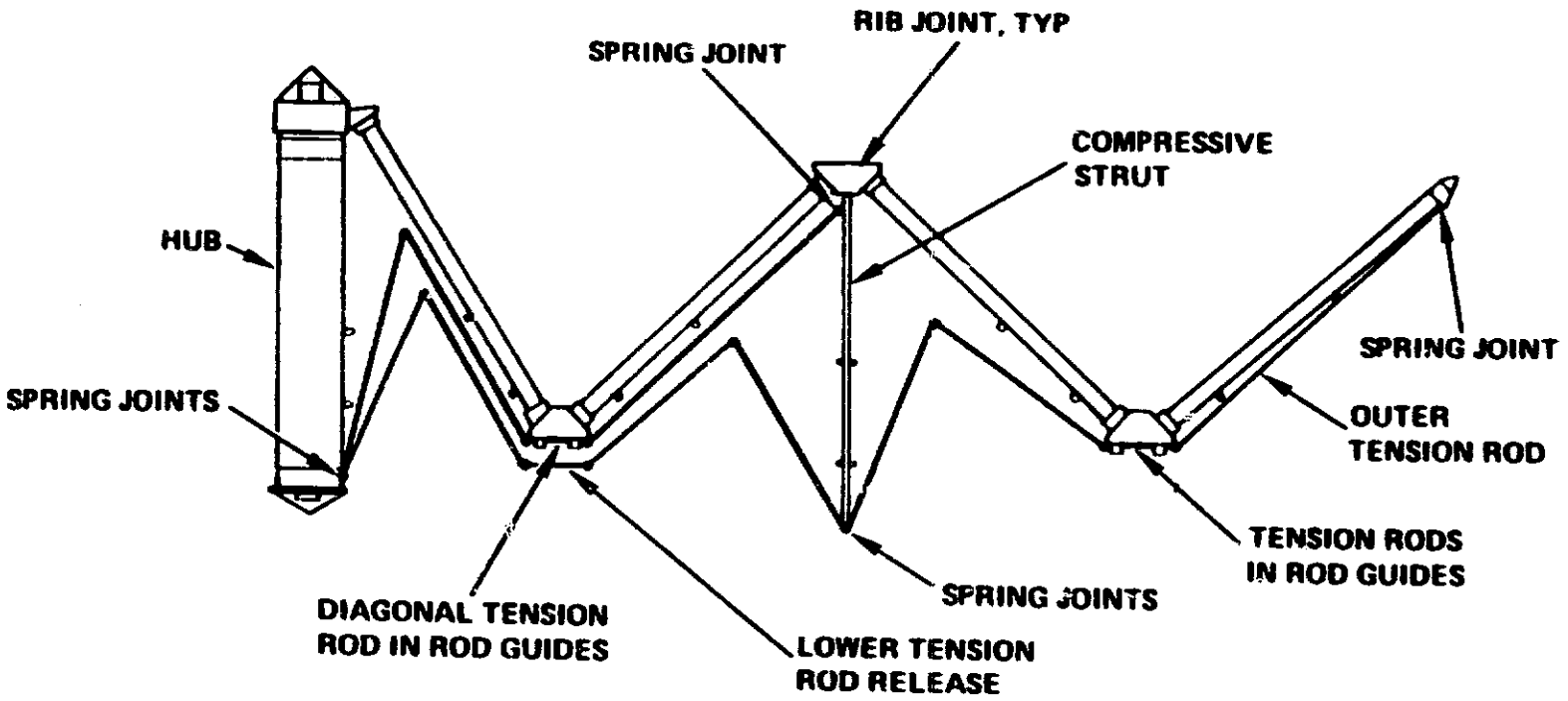

Ford Aerospace & Communications Corporation

FIGURE 3.4-3. DTS STOWED REFLECTOR (SHOWN WITHOUT MESH)

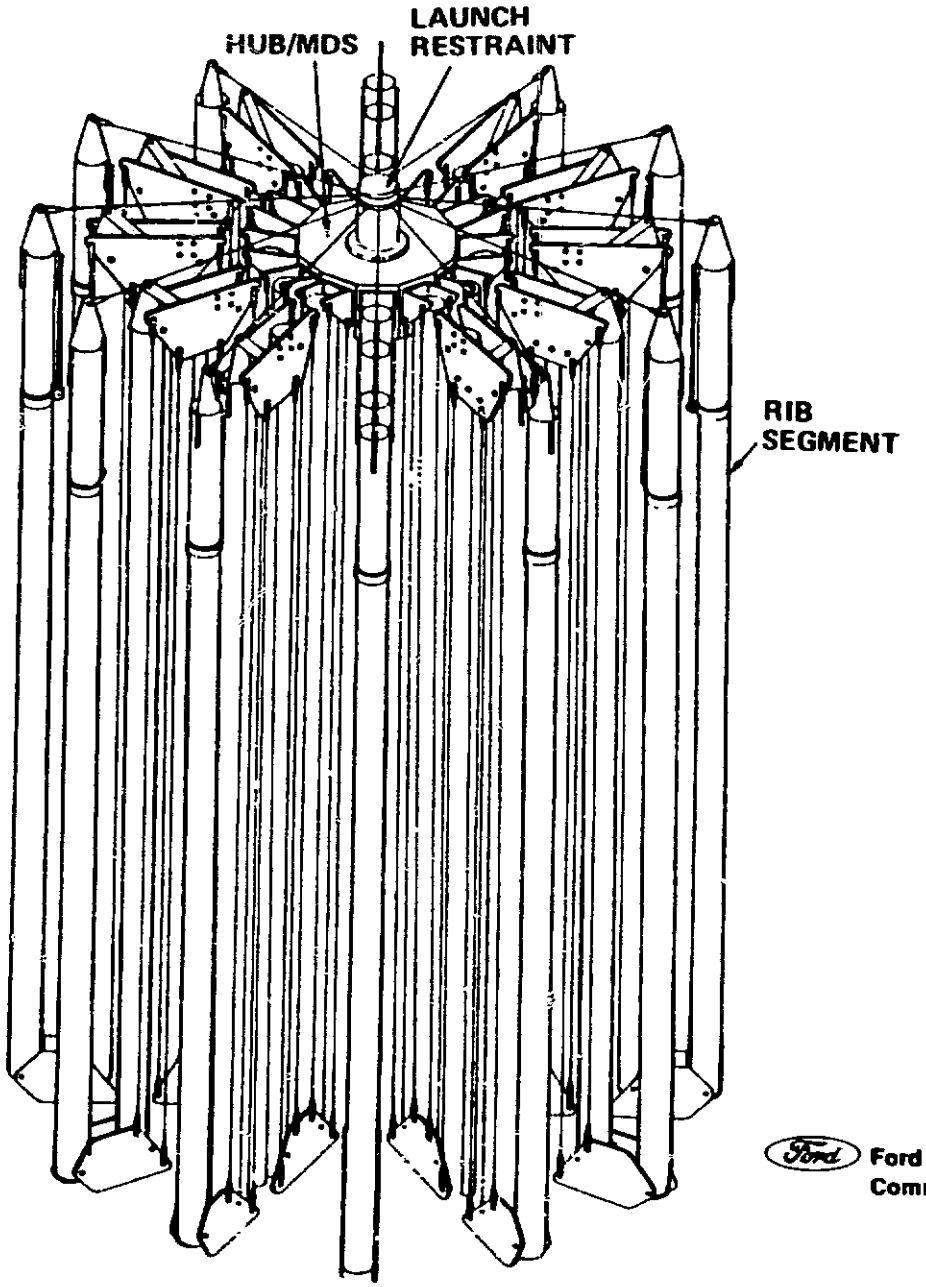

Ford Aerospace & Communications Corporation

members by the four bar-linkage. Tension rods are pulled free from the tension rod guides and clips by the rib action. Linkages drive the ribs to their deployed positions simultaneously. Once fully deployed with the inner and outer rib joints latched, the rib assumes the characteristics of a pinned-end truss.

3.4.3 Reflector Mesh Concept

The surface design used on the DTS structure is a Harris pioneered, dual drawing surface system. The design involves the placement of a secondary structure behind the primary reflective surface and joining the two with a number of ties sufficient to achieve the desired surface accuracy.

The implementation of this surface involves the use of a gold plated mesh to form the reflective surface, multistrand graphite cords to create the surface contour, graphite-epoxy strips to establish gore boundaries, and adjustable standoffs by which the reflective surface assembly is attached to the graphite radial ribs. The reflective mesh is a .0012 inch diameter gold plated molybdenum mesh knitted into a tricot pattern with openings small enough to provide a reflective surface at UHF. Harris developed this mesh and was the first to use preplated, molybdenum monofiliment wire and the first to use a tricot knit for a RF reflective surface. Molybdenum with its high strength, low coefficient of thermal expansion, and excellent plating characteristics results in a highly reflective surface with relatively low tensions, good resistance to handling, and minimal thermal interaction with the graphite cord and graphite rib supporting structure. Preplating with gold assures minimal interfilament friction with uniform, optimum thickness for RF reflectivity. The tricot knit is most familiar as the double-knit fabrics

that were popular for their ability to "give" in two directions without unravelling at the edges or with broken strands.

Multistrand graphite cords are used to form a thermally insensitive substructure which combines with GFRP ribs to form a precision foundation for the mesh. The circumferential arrangement of cords increases the effective resistance of the ribs to axisymmetric loading produced by thermally induced mesh tension variations. The negative thermal properties to produce a near optimum condition for thermal stability.

4.0 SPACECRAFT POWER, MASS and DISSIPATION

4.1 Electrical Power Subsystem

4.1.1 Requirements

The electrical power subsystem must generate, store, condition and distribute electrical power to ensure the spacecraft meets all performance requirements throughout all mission phases. Specifically, operation in sunlight at 2395 watts (see Table 4-1.1 and 4.1-2) and bus subsystem maintenance in eclipse of 1266 watts is required.

4.1.2 General Description

The spacecraft electrical power subsystem (EPS) is a dual bus, direct energy transfer system designed to accommodate a spacecraft primary load of approximately 2.4 kW for a 10 year equinox synchronous orbit lifetime. Primary power is provided by two separate Sun-oriented planar solar array wings. The voltage of each solar array wing is regulated by a separate sequential linear partial shunt regulator. During periods of solar eclipse and peak requirements, power is supplied by two nickel hydrogen batteries. These batteries supplement the solar array during peak power demands such as augmented catalytic thruster (ACT) firings. DC/DC converters provide regulated power to secondary loads. The inter-relationship of the major EPS elements is illustrated in Figure 4.1-1.

The solar array consists of two single axis Sun-oriented wing assemblies. Each assembly consists of a deployment mechanism, three rigid

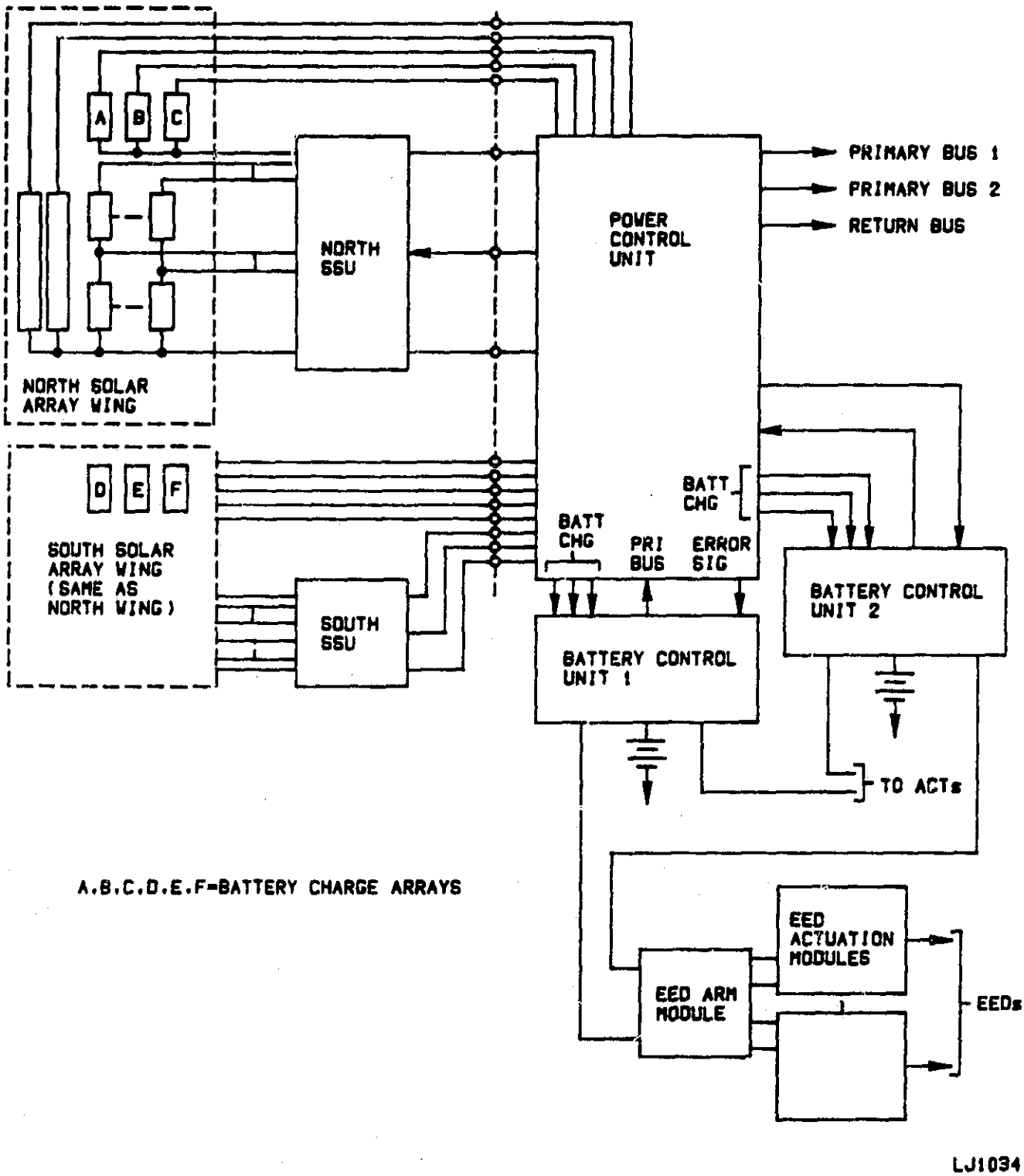

KEL50039/CA1
1-23-85/GM/MISC1

FIGURE 4.1.1 ELECTRICAL POWER SUBSYSTEM

panels and an orientation mechanism connected to the solar array drive system. The solar array drive assembly (SADA) consists of a dual, two channel solar array drive electronics (SADE) and two solar array drive mechanisms. The drive provides for the support and positioning of the arrays about the satellite pitch axis and for the transfer of power and signals from each array to the satellite module.

TABLE 4.1-1

Communication Payload DC Power Requirement

	Watts
UHF	
o High power amplifiers (24) @ 20.8 watts RF each = 500 watts RF efficiency = 30% 500/.30 =	1667.0
o Downlink RCVR/Translators (25) @ 6W	150.0
o Uplink RCVR/Translators 25) @ 6W	150.0
Total UHF	1967.0
Ku-Band	
o Upconverters @ 3W	3.0
o Downconverters @ 3W	3.0
o TWTA (1) @ 10W RF efficiency = 30% 10/.30 =	33.3
o Upconverter L.O. @ 3W	3.0
o Downconverter L.O. @ 3W	3.0
Total Ku-Band	45.3
Payload Total	2042.3

TABLE 4.1-2
Power Summary

Watts at beginning of synchronous orbit (BOL)

	SYNCHRONOUS ORBIT		
	AUTUMNAL EQUINOX	SUMMER SOLSTICE	ECLIPSE
COMMUNICATIONS TRANSPONDER	2042.2	2042.2	1021.2
RF TELEMETRY, TRACKING & COMMAND	16.8	16.8	16.8
PAYLOAD SUBTOTAL	2059.0	2059.0	1038.0
SPACECRAFT CONTROL ELECTRONICS S/S	69.0	69.0	69.0
ATTITUDE CONTROL SUBSYSTEM	95.6	95.6	45.6
PROPULSION SUBSYSTEM	0.7	0.7	0.7
THERMAL CONTROL	92.0	92.0	46.0
ELECTRICAL POWER SUBSYSTEM	13.0	13.0	10.0
HARNESS LOSS	21.3	21.3	15.0
BUS SUBTOTAL	291.6	291.6	186.3
BATTERY INTERFACE LOSS	- -	- -	41.9
BATTERY CHARGING	101.9	44.9	- -
SATELLITE TOTAL	2452.5	2395.5	1266.2
SOLAR ARRAY CAPABILITY	3575.0	3251.0	- -
BATTERY CAPACITY AT 70% DOD 2-36.8 Ah NiH2 TYPE BB (36.8)	- -	- -	1502.7
MARGIN	1122.5	855.5	236.5
% MARGIN	46%	36%	19%

Watts at the end of 10 years (EOL)

COMMUNICATIONS TRANSPONDER	2042.2	2042.2	1021.2
RF TELEMETRY, TRACKING & COMMAND	16.8	16.8	16.8
PAYLOAD SUBTOTAL	2059.0	2059.0	1038.0
SPACECRAFT CONTROL ELECTRONICS S/S	69.0	69.0	69.0
ATTITUDE CONTROL SUBSYSTEM	95.6	95.6	45.6
PROPULSION SUBSYSTEM	0.7	0.7	0.7
THERMAL CONTROL	92.0	92.0	46.0
ELECTRICAL POWER SUBSYSTEM	13.0	13.0	10.0
HARNESS LOSS	21.3	21.3	15.0
BUS SUBTOTAL	291.6	291.6	186.3
BATTERY INTERFACE LOSS	- -	- -	37.6
BATTERY CHARGING	105.4	45.3	- -
SATELLITE TOTAL	2456.0	2395.5	1261.9
SOLAR ARRAY CAPABILITY	3578.0	2828.0	- -
BATTERY CAPACITY AT 70% DOD	- -	- -	1502.7
MARGIN	622.0	432.1	240.8
% MARGIN	25%	18%	19%

The SADE is a dual box containing two redundant sides. Each of these sides is capable of controlling both channels of the solar array drives. The solar array drive has a stepper motor with two independent motor windings for redundancy.

The SADA always provides drive motion at the rate of one step (0.1125°) of each array, every 27 seconds. This corresponds to an angular rate of 15°/hour for each array. In addition to this stepping rate, a slew augmentation capability is provided to speed up the operation of each or both the north and south arrays at a slew rate consistent with dynamic constraints. The direction and number of slew steps are commandable from the ground.

During the transfer and drift orbits, the array is stowed so that load support and battery charging are accomplished with the two outboard panels (one per wing). The array is designed to support synchronous orbit operation at end of life summer solstice with an electrical power capacity of 2828 W.

The battery configuration consists of two nickel hydrogen batteries connected to the applicable bus through battery discharge diodes. The battery charge current is controlled by dedicated solar array sections and battery charge controllers. The charge current is applied sequentially to each battery on a 50% duty cycle. Open circuit protection is provided for the batteries by diode bypass networks connected across each cell. Temperature and pressure sensors are utilized to provide temperature control inputs for battery heaters and sense the state of charge of the cell.

The power control electronics (PCE) consists of the power control unit (PCU), two shunt dissipator assemblies, two battery control units, and electroexplosive device actuation functions. A key feature of the PCE is the provision of two independent primary buses. The outputs of each solar array wing and one battery are dedicated to each bus, with the capability provided to parallel connect or separate the two buses by ground command, as required. The output of each solar array wing is independently regulated to 35 $\pm$ 0.5 V DC by use of a sequential linear partial shunt regulator. The PCE provides sequential battery charge control and individual battery reconditioning capability by ground command. Single part failure criticality is eliminated by use of circuit redundancy and alternate modes of operation are selectable by ground command. All satellite electroexplosive devices (EEDs) are controlled by the PCE, which employs redundant, fail safe circuitry for these important functions.

4.1.3 Solar Array

The solar array design relies extensively on already developed and flight-proven hardware from the INTELSAT V program. The solar array design for MSS would be modified to utilize improved efficiency cells.

The solar array consists of six deployed solar cell panels arranged in two identical wings. Each wing consists of three solar panels, holddown/release mechanism, deployment mechanism, and a yoke, complete with hinge for mounting to the spacecraft solar array drive mechanism. The array blocking diodes are mounted in the sequential shunt assemblies, mounted on the inboard solar panel.

Each wing of the array has an output of 1414 W nominal at 35 V at the PCU terminals at summer solstice after 10 years in orbit. This is accomplished on each panel by 58 parallel by 99 series, 20 X 40 mm solar cells, each covered with a 150 micron thick ceria-doped microsheet cover slide. Each of the three solar panels composing one wing is 2.1 X 2.5 m. The panel substrates are fabricated from graphite face sheets bonded to an aluminum honeycomb core as used for INTELSAT V.

The overall width is 2.1 m and deployed length is approximately 8.75 m including the yoke and mounting hinge. The solar array wing accommodates 17,226 solar cells for the primary power and 567 cells for battery charging. Blocking diodes on the main bus form part of the shunt dissipator assembly.

The array is stowed during launch and transfer orbit. Load support and battery charging are accomplished with two outer panels (one per wing). Power available at BOL equinox is 3575 W. The array is designed to support synchronous orbit operation at EOL equinox with an electrical power capacity of 3078 W.

4.1.4 Battery Design

Two nickel-hydrogen batteries are connected to the applicable bus through the battery control units. Each battery consists of 27 hermetically sealed cells connected in a series that deliver a nominal discharge voltage of 33.6 V and a minimum capacity of 36.8 Ah at 10°C measured to 1.0 volt per cell.

The batteries will be similar to those flying in INTELSAT V Flight Models 6, 7, and 8, the only flight-proven Ni-H_2 spacecraft to date.

The nominal mass of the batteries is 56.3 kg. Thermal control is achieved with individual resistive heaters for each cell, which are operated by the heater control circuit in the battery control units based on temperature sensed by a precision thermistor mounted on the battery. Two additional thermistors serve as telemetry sensors.

The electrical design is implemented with the required redundancy and reliability. The series connection between cells is provided by two parallel connected wires. Battery power connections are made to the terminals at the ends of the cell series with four redundant wires leading to the battery connector. The battery is protected against an open circuit condition by a diode bypass network connected across each cell. Battery charging is provided by dedicated solar array sections and battery charge controllers in the battery control units. This configuration permits multiple charge rate combinations that result in excellent flexibility and reliability.

The batteries can be utilized to a 70% depth of discharge, based on the actual capacity measured at 10°C.

Table 4.1-3 summarizes key battery performance requirements and capabilities.

4.1.5 Power Control Electronics

The power control electronics consists of the following elements:

1 each - sequential shunt assemblies

1 each - power control unit

2 each - battery control units

1 each - electroexplosive device control function

The sequential shunt units are a direct adaptation of INTELSAT V units modified for mounting in the solar array yokes.

TABLE 4.1-3. Major Battery Requirements vs. Capability

Item	Requirement	Capability
Battery load power (EOL)	1262 W	1500 W**
Battery life	10 years	10 + years
Battery voltage (EOL)	27.8 V min	33.6 V
Battery depth of discharge	70% max	70.0%
Battery cycles charge/discharge	880 cycles	1000 + cycles
Cell failure protection	Open circuit protection	Diode bypass circuit
Temperature range control	0°C to 25°C	Heater + charge rate control

** End of life with no cell failures

The power control unit is greatly simplified over INTELSAT V for this topology. Battery control functions and EED functions are contained in the Battery Control Units and EED Control Unit respectively.

Solar Array Regulation

The power control unit in conjunction with the two sequential shunt units (SSU) regulate the voltage output of the solar array. This is accomplished by each SSU sequentially shunting the voltage taps (control buses(of the main array subcircuits of each wing as required to maintain the primary bus voltage of 35 ± 0.5 V DC during sunlight operation. Sequential shunt operation is controlled by a primary bus voltage error amplifier located in the PCU. The same error signal from the error amplifier also controls operation of the following:

- Solar array power reduction control
- Battery voltage limiters located in the battery control units
- Battery charge controllers located in the BCUs

Use of the existing INTELSAT V sequential shunt units allow control of bus regulation at beginning of life. The lower load limitation results from the two unregulated (unshunted) main power sections of each solar array wing. To reduce the minimum spacecraft load to solar eclipse load, the two unregulated array power sections of each solar array wing are sequentially switched off the buses as loads are reduced. This is accomplished through the solar array power reduction control located in the PCU. When the error signal moves

outside the range for maximum solar array voltage regulation this signal causes the solar array power reduction control to open circuit the unregulated solar array unregulated power circuits on each solar array wing as required. The resulting reduction of solar array output allows bus regulation to be maintained. As primary bus loads are increased, full solar array power commands applied to the solar array power control reconnect the full solar array capability. In the event that primary bus loads are increased to nearly design limits prior to initiating the above command the batteries will support the power deficiency until the command execution.

Eclipse Load Support

Upon entrance into solar eclipse the error signal from the error amplifier will move outside the range for minimum solar array voltage regulation. This change as sensed by the battery voltage limiter in the battery control unit (BCU) causes activation of the battery voltage limiter. Battery voltage upon eclipse entrance may be as high as 42 V. The voltage limiter will provide the required voltage drop to maintain the primary bus voltage below 35 V. As the battery discharge voltage approaches 35 V, this limiter will provide a low loss battery power transmission path for the remaining eclipse duration. Upon exit from solar eclipse restoration of solar array power will deactivate the battery voltage limiter.

This same voltage limiter is utilized in sunlight to limit the maximum voltage applied to ACT heaters to 35 V. Upon commanding on ACT heater the battery voltage limiter will operate under local loop control independent of the primary bus error signal. Control of voltage applied to these heaters is similar in function as with the primary bus.

Battery Charge Control

Battery charge control is provided by the following:

- o Solar array battery charge circuits
- o Battery charge controllers in the BCUs
- o Battery charge circuit relays

Three battery charge circuits on each solar array wing are connected in series with the solar array buses within the sequential shunt units. This configuration provides three current sources from each solar array wing.

These battery charge circuits are connected to the BCU via the PCU. Within the BCUs, these circuits are connected to the batteries via charge on/off relays and charge controllers. Provided in each BCU is a relay to parallel the A and D and the B and E solar array battery charge circuits. Required battery charge rate is selected by use of the charge on/off relays and circuit parallel relays. Continuous battery trickle charge is maintained by closure of the circuit C and F relays in the respective BCUs. Full charge at the required level is selected by closure of the A, B, D, E relays and the circuit parallel relays.

Sequenced operation of the battery charge controllers will allow alternate full charge of one battery while the other battery is maintained in trickle charge.

Battery charge controllers in each BCU are key to providing the required charge control.

Upon eclipse emergence the battery charge controllers are inhibited until the primary bus error signal approaches a level indicating that the solar array is in voltage regulation. This function automatically ensures that the battery charging load is not applied to the solar array bus until ability to support spacecraft loads is provided.

Battery Temperature Control

Control of minimum battery temperature is provided by heaters in each battery controlled by battery temperature controllers in the BCUs. This controller design remains the same as used in the INTELSAT V PCU. A thermistor in each battery provides the temperature sensing for control. Control limits for battery heater operation are as follows:

Heater on $(+1)^{\circ}C$

Heater off $(+5)^{\circ}C$

Command inputs are provided to override the automatic temperature control function. Through these inputs the battery heaters can either be inhibited or turned on independent of the automatic controller operation.

Telemetry Monitors

Conditioning of analog and binary telemetry data generally is accomplished within the EPS. The only exception will be temperature monitors where the thermistor connections will be passed through for processing in the

telemetry unit. Design of the conditioned telemetry monitors remain the same as INTELSAT V. These monitors are as follows:

a. Current Telemetry

b. Battery Cell Voltage (multiplexed)

c. Bus and Battery Voltage

d. Status Monitors

E. Battery Cell Pressure

All analog signal conditioning monitors will provide a 0 to 5 V output. Status monitors will provide or TTL compatible output.

Battery cell pressure monitor outputs will be provided as separate analog channels and will not be multiplexed with battery cell voltages.

4.1.6 DC/DC Converters

The DC/DC converters are the electrical interface between the majority of spacecraft loads and the primary power buses. The converters provide load control, fault isolation, and optimized management of secondary load power. By locating the DC/DC converters within the user load unit, electromagnetic compatibility (EMC) and secondary power regulation are optimized.

4.1.7 Power Budget and Performance

The power summary for synchronous orbit conditions is presented in Table 4.1-1. The summary shows predicted values of load power by subsystem,

the predicted solar array performance at the end of 10 years, and the resulting system power margin.

4.2 Spacecraft Dissipation Summary

The MSS baseline communication payload dissipation is 1600 watts under worst case signal conditions. Bus module dissipation is approximately 375 watts for a satellite total thermal dissipation of just under 2000 watts. The FACC bus has been sized to accommodate 2100 watts of communications module dissipation and 500 watts of service module dissipation. A breakdown of the dissipation summary can be seen in Table 4.2-1.

The primary dissipators on this design are the north and south panels which radiate directly into space. This provides the most direct heat path. Heat rejection is provided by OSR second-surface mirror radiator surfaces utilizing metalized quartz glass.

Section 5.1 and 5.2 will discuss the structure and thermal configuration.

TABLE 4.2-1
Dissipation Summary

Watts at beginning of synchronous orbit (BOL)

	SYNCHRONOUS ORBIT		
	AUTUMNAL EQUINOX	SUMMER SOLSTICE	ECLIPSE
COMMUNICATIONS SUBSYSTEM	1542.3	1542.3	771.2
RF TELEMETRY, TRACKING & COMMAND	16.8	16.8	16.8
BUS COMPONENTS	16.6	16.6	12.0
COMM HARNESS LOSS	20.5	20.5	15.0
PAYLOAD MODULE SUBTOTAL	1596.2	1596.2	814.9
SPACECRAFT CONTROL ELECTRONICS S/S	58.0	58.0	58.0
ATTITUDE CONTROL SUBSYSTEM	90.0	90.0	40.0
PROPULSION SUBSYSTEM	0.7	0.7	0.7
THERMAL CONTROL	80.0	80.0	40.0
BUS HARNESS LOSS	7.5	7.5	6.6
SHUNT CONTROL UNIT	111.4	101.7	5.0
BATTERY CONTROL UNIT	8.0	8.0	8.0
BATTERY INTERFACE LOSS	- -	- -	37.6
BATTERY DISSIPATION	34.2	36.4	286.7
BUS MODULE SUBTOTAL	389.8	382.3	482.6
SATELLITE TOTAL	1986.0	1978.5	1297.5

Watts at the end of 10 years (EOL)

COMMUNICATIONS SUBSYSTEM	1542.3	1542.3	771.2
RF TELEMETRY, TRACKING & COMMAND	16.8	16.8	16.8
BUS COMPONENTS	16.6	16.6	12.0
COMM HARNESS LOSS	18.6	18.6	15.0
PAYLOAD MODULE SUBTOTAL	1594.3	1594.3	815.0
SPACECRAFT CONTROL ELECTRONICS S/S	58.0	58.0	58.0
ATTITUDE CONTROL SUBSYSTEM	90.0	90.0	40.0
PROPULSION SUBSYSTEM	0.7	0.7	0.7
THERMAL CONTROL	80.0	80.0	40.0
BUS HARNESS LOSS	7.3	7.3	6.3
SHUNT CONTROL UNIT	93.8	86.4	5.0
BATTERY CONTROL UNIT	8.0	8.0	8.0
BATTERY INTERFACE LOSS	- -	- -	37.6
BATTERY DISSIPATION	34.5	36.4	292.7
BUS MODULE SUBTOTAL	372.3	367.1	488.3
SATELLITE TOTAL	1966.6	1961.4	1303.3

The power summary presents the worst case power requirements of each subsystem. At the end of 10 years in orbit, the electrical power subsystem will supply 2828 watts during sunlight hours. The power required for full spacecraft operation during sunlight is only 2395.9 watts for a total margin of 432.1 watts.

The FACC bus can provide sufficient power for the second generation MSS.

4.3 Spacecraft Mass Summary

The spacecraft mass has been minimized to provide a maximum mass margin. The calculated mass margin of 93 kg represents 8% of the spacecraft dry mass. Secondly, extensive calculations have been performed to develop accurate mass estimates for the spacecraft items. The spacecraft mass summary can be seen in Table 4.3-1. Note that with a Thiokol Cap. PSM 63E perigee stage motor deployed from STS cargo bay, the perigee motor capability is 1247.4 kg (0° motor off-load and 15% perigee augmentation). Table 4.3-2 represents our rough estimate of STS cargo mass of the MSS IPSM motor perigee stage for a typical shuttle launch. Table 4.3-3 provides a mass comparison between the LMSC and Harris Corp. reflector and deployment boom.

conclusion is that the FACC bus can support the predicted mass and launch on STS.

TABLE 4.3-1

Mass Summary

(Single LMSC Reflector and Boom)

SUBSYSTEM	MASS (kg)	MASS TOTAL (kg)
Payload		382.5
o Transponder, UHF	144.1	
o Transponder, Ku-Band	59.2	
o 20.0 m Reflector (60 @ 900 MHz LMSC w/ 20% margin)	107.3	
o One UHF Feed	70.0	
o 0.4M Ku-Band Reflector	1.0	
o Ku-Band Feed	.9	
TT&C		23.5
AOCS		69.9
Propulsion		141.2
Power		163.6
o Solar Array - 2828W EOL 10 years	88.9	
o Batteries 2-36.8 Ah, Ni-H_2, 50% eclipse ops.	56.3	
o Miscellaneous	18.4	
Structure		264.0
o Main Body	156.0	
o 1 Reflector Deployment Mechanism (LMSC) (incl. 20% margin)	108.0	
Thermal		35.7
o OSR and Insulation	7.8	
o Heat Pipes	27.9	
Electrical Integration		51.0
Mechanical Integration		14.8
Margin		93.1
Dry Spacecraft Total		1239.3*

* An IPSM 63E perigee stage capability is 1247.4 kg (0% offload of motor, 15% perigee augmentation)

TABLE 4.3-2

Mass for STS Mission with IPSM-63E Perigee Motor

	MASS (kg)
Spacecraft EOL Mass	1247.40
Stationkeeping and Drift Orbit Propellant	326.12
Apogee Propellant	1268.57
GTO Mass	2842.09
Perigee Augmentation (15%)	366.10
Post Perigee Maneuver	3208.20
Perigee Stage Burnout Mass	459.22
Perigee Propellant	4066.00
Spin-up and Attitude Control	6.00
Deployed Mass	7739.42
ASE Mass	860.44
Cargo Mass	8599.86

Table 4.3-3. LMSC vs. Harris Reflector System Mass

	LMSC			Harris		
		MASS (kg)			MASS (kg)	
	Qty	Each	Total	Qty	Each	Total
o Reflector, 20 m	1	107.3	107.3	1	181.4	181.4
o Deployment Boom	1	108.0	108.0	1	227.0	227.0
o Single Reflector System			215.3			408.4
o Reflector, 20.0 m	2	107.3	214.6	2	181.2	362.4
o Deployment Boom	2	108.0	216.0	1	454.0	454.0
o Dual Reflector System			430.6			816.4

4.4 Spacecraft Life and Redundancy Considerations

The FACC design uses previous heritage hardware that has been qualified for a 10 year mission. New hardware is derived from current technology of the minimum risk and highest reliability. This approach to the design selection minimizes reliability risks for MSS Satellite.

The key reliability features of the design are:

- o All electronics units are redundant
- o Dual power buses allow for degraded system operation in the event of a bus failure
- o Open cell protection for all nickel-hydrogen battery cells
- o Bipropellant apogee thruster ensuring higher reliability then conventional solid fuel apogee motors

Component level redundancy and extensive cross-strapping are used throughout the design to eliminate single point or critical failure modes. Most spacecraft failure effects are isolated to individual subsystems or limited to lower level subsystem equipment groups so that a failure will not disable or degrade the performance of the remainder of the spacecraft or redundant functional units.

The primary mode of switching of redundant spacecraft equipment is by relay activation. All switching to standby redundant equipment is performed by ground uplink command. This approach is used instead of onboard failure detection to avoid false switching and undesirable spacecraft operation.

Degraded or failed components are primarily detected by monitoring telemetry and spacecraft performance.

5.0 Needed Modifications

5.1 Structure Modifications

The FACC bus structure can accommodate the single reflector design as seen in the power. dissipation and mass summaries in sections 4.1, 4.2 and 4.3, respectively.

No major modifications to the structure are required. For detailed spacecraft structural configuration, see Section 3.4.

An overview of the spacecraft structure is as follows:

Bus Module System

- Propulsion - Subsystem provide sufficient impulse for 10 year of on-orbit attitude control. The liquid bipropellant nitrogen tetroxide (N_2O_4), monomethylhydrazine (MMH) subsystem uses one titanium oxidizer tank (located at C.G. of S/C) and two tanks for MMH, all pressurized by two tanks of helium. This subsystem will provide final injection into geosynchronous orbit and allow totally redundant attitude control forces. In addition, the attitude and orbit control thrusters provide nutation control, initial spacecraft despin, apogee, impulse, attitude control and stationkeeping attitude control. Redundant thruster systems are isolated by sets of fuel and oxidizer latch valves.

Fuel and Oxidizer Latch Valves

- Power - The dual bus direct energy transfer electrical power subsystem, in conjunction with the solar arrays and solar array drives provide electrical power for the satellite. Two 36.8-ampere-hour nickel hydrogen batteries provide power for the satellite during eclipses and the solar array for peak transient loads.

- Attitude Control - The subsystem design is a momentum-bias type with two momentum wheels. A reaction wheel is provided for redundancy during three axis satellite control. Attitude information is provided by earth and sun sensors, which are used both in transfer orbit and synchronous orbit operations.

- TT&C - The TT&C uplink signals, with command or ranging information modulated onto a carrier, are received by the command antenna and fed to redundant receivers. The uplink signal is demodulated, providing the command signal to the command units or the range tone signal to the telemetry transmitter for turn-around ranging. The command signals are detected and processed by the command unit. The ranging tones from the receiver are fed to the telemetry transmitter, where they phase modulate the downlink carrier.

Payload Module System

- Optimized Structure - The structure subsystem provides support and housing for the payloads and all supporting subsystems, and mates with the perigee stage. It provides the major satellite thermal control functions.

- Solar Array and Drive - The solar array subsystem (as described previously) is composed of two wings, three panels per wing, containing two separate electrical buses. The solar array fully deployed tracks the sun by the solar array drive (SADA) of the attitude and orbit control subsystem.

- Thermal Control - See Section 5.2

- Modularity - The spacecraft is composed of modules. The ability to integrate and test the modules separately has proven to be of tremendous value. The value is seen in reduced schedule risk and providing test advantages.

5.2 Thermal Control Modifications

Thermal Control is accomplished by primarily passive techniques (selective component location, selective finishes, and materials, multilayer insulation) to maintain the satellite equipment within acceptable temperatures. Heaters augment the passive design for components requiring unique temperature control.

The maximum thermal dissipation of the MOS payload module (1600 watts) is lower than the maximum thermal capability (2100 watts) of the FACC bus. The average predicted temperature of the payload module meets the internally imposed requirements. Therefore, no modifications to the thermal control subsystem are required.

The FACC bus thermal design combines both traditional and new concepts for 3 axis spacecraft. The thermal radiators are located on the north and

south panels as was mentioned in Section 4.2. Heat pipes are used on the north and south panels of the payload module to transfer heat to colder locations within the module. The aluminum/ammonia variable conducting heat pipes embedded into the honeycomb north and south panels, are not redundant, but their heat transport is derated 50% relative to the performance requirements. The heat pipes are straight, U-shaped and L-shaped with a maximum operating temperature of +50°C.

5.3 Solar Pressure Effects for MSS - Configuration B1

Due to the size and complexity of the MSS satellite, initial calculations of solar pressure effects were confined to modelling major parts of the structure for input to simple calculations. An accurate and thorough solar pressure model is beyond the scope of this current effort. The procedure to be followed for future analytical efforts is outlined here for reference.

1. Model each major segment such that data may be entered into the solar pressure computer program.

2. Investigate modelling techniques for parabolic reflectors, specifically the "polyconic parabolic" approximation.

3. After entering the data, run the program for a variety of orbital and seasonal cases.

Consideration of the B1 configuration has shown the following points:

1. CG location in the y direction is critical - zero offset is assumed.

2. Symmetry of the various structural parts with respect to the y-z plane is also also critical to keeping roll/yaw torques small. In other words, there are no momentum arms with y subscripts in Figure 5-1.

3. Peak torques will appear about the y axis and thus will drive momentum wheel size and wheel operating range.

4. During the day, pitch torque will vary sinusoidally according to the sketch in Figure 5-2. Peak torque is estimated as 3.8×10^{-4} Nm. This means a pitch momentum wheel needs to absorb about 12 Nms momentum over 1/2 a day.

5. Roll/Yaw torque will occur when the sun rises out of the equatorial plane, this angle peaks at 23.44 degrees. To give a rough idea of magnitude, the major segment of the support structure was analyzed. The triangular structure was examined and found to exhibit an area that ranges from 4.8 ft^2 per bay up to 7.4 ft^2 per bay depending on the sun angle out of equatorial plane.

Using the maximum, a cylindrical model was generated. This section at midnight in summer solstice, would contribute 5.5×10^{-5} NM of torque about the roll axis. Based on pitch torque values for various segments, the other segments contribution to roll/yaw torque could at most triple this value. For sizing purposes, a peak roll/yaw torque level of 1.5×10^{-4} Nm seems appropriate. Based upon this preliminary analysis, it was indicated that the existing attitude control subsystems in the FACC bus can handle the solar pressure effect caused by the large size reflector and the deployment boom.

The analysis also indicated that FACC buss can achieve the required pointing accuracy with a single antenna configuration.

FIGURE 5.1 CONFIGURATION B1 SOLAR TORQUE MODEL WITH MOMENT ARMS

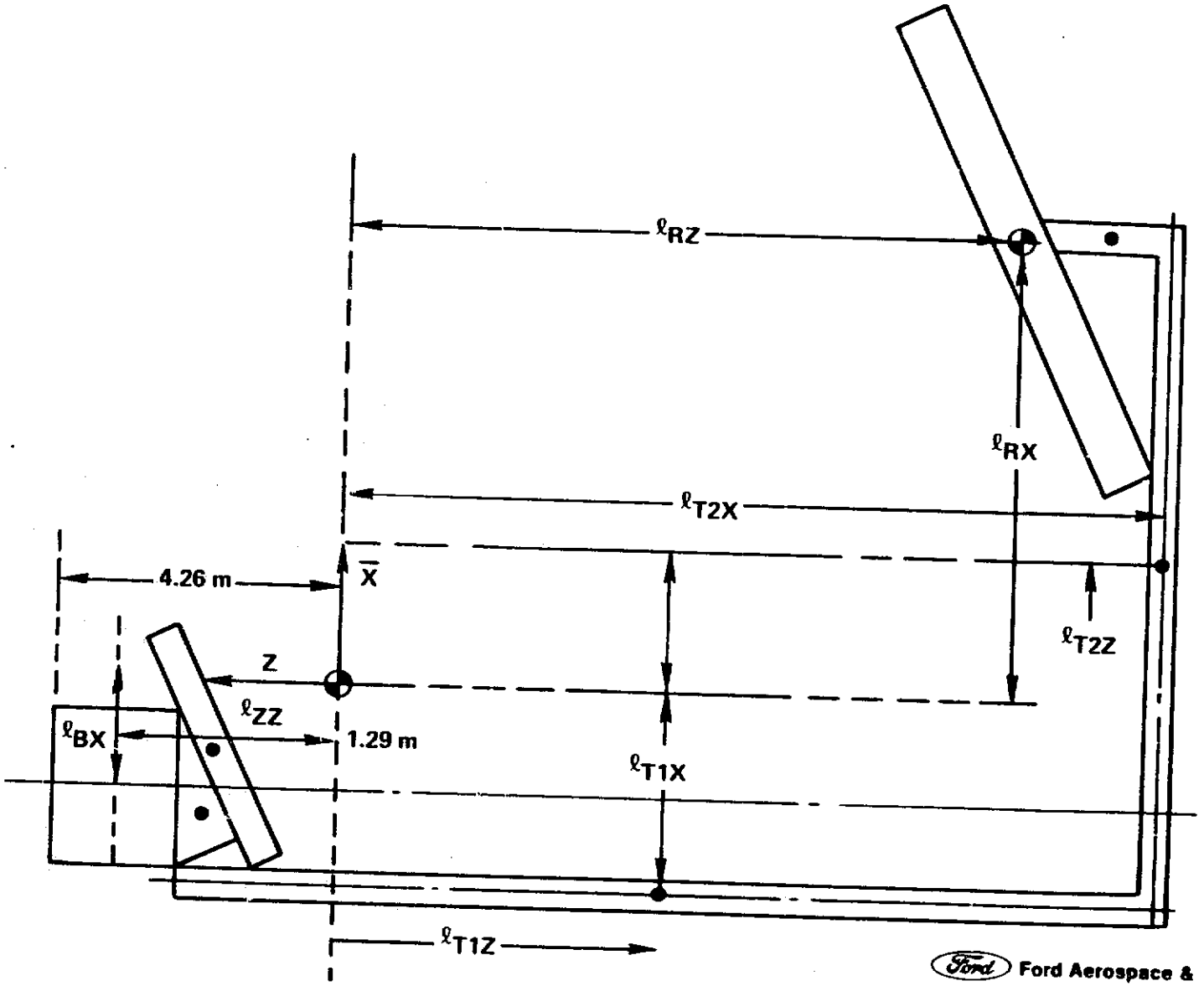

Ford Aerospace & Communications Corporation

FIGURE 5.2. LMSS PITCH SOLAR PRESSURE TORQUE

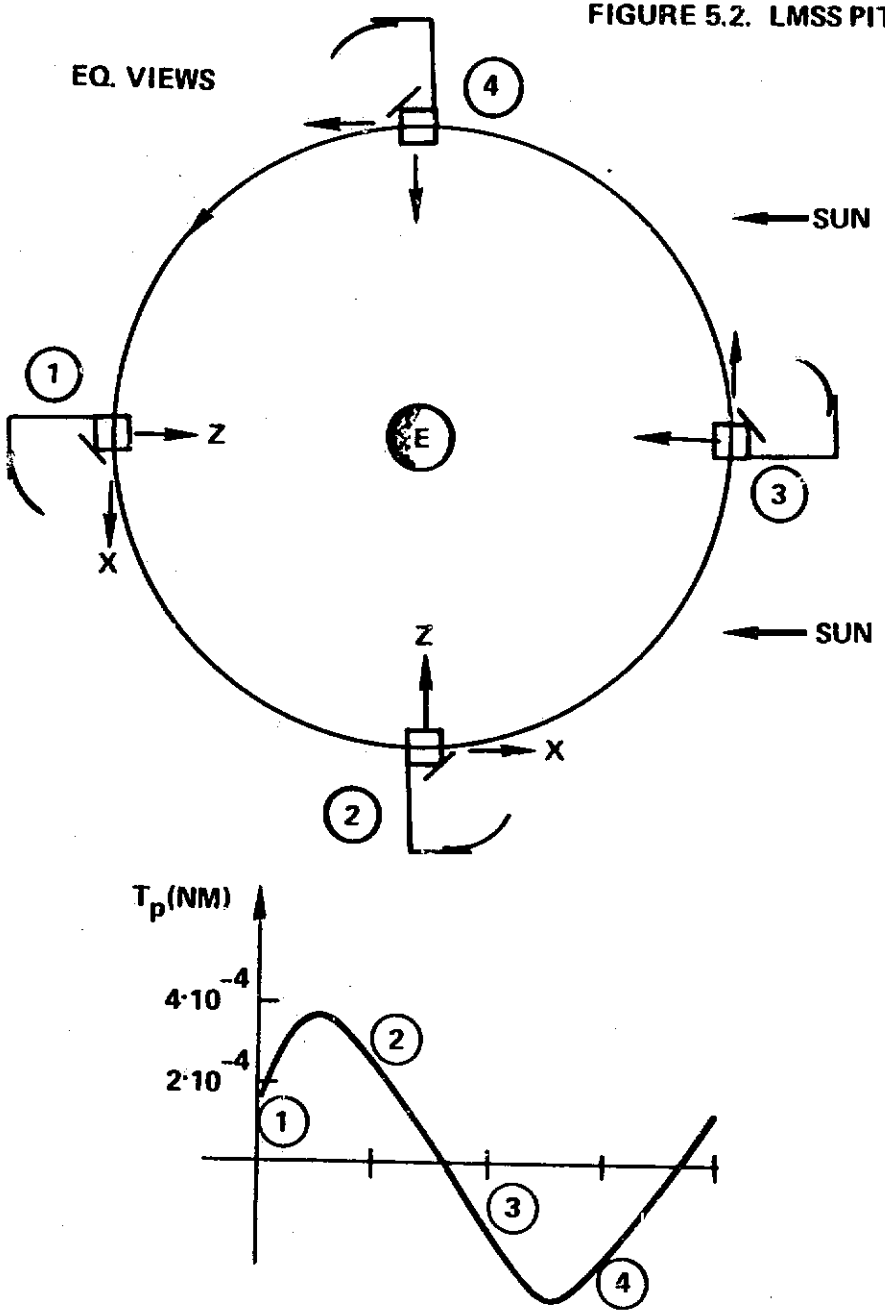

VIEW 1
12:00 MIDNITE

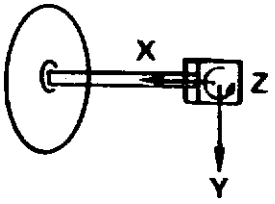

+Y TORQUE

VIEW 2
6:00 AM

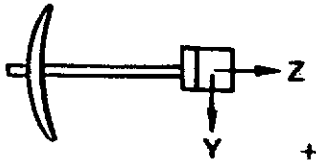

+Y TORQUE

VIEW 3
12:00 NOON

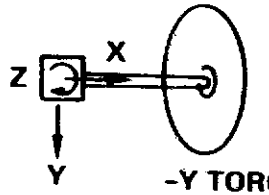

-Y TORQUE

VIEW 4
6:00 PM

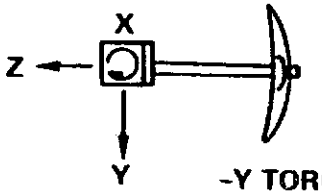

-Y TORQUE

Ford Aerospace & Communications Corporation

6.0 ANTENNA FEED STUDY

6.1 Antenna Configuration

The antenna configuration selected is shown in Figure 6-1. This is a dual frequency transmit and receive antenna and was selected for the typical spacecraft reasons i.e., weight, space, and cost. Further, this simplifies the design in spacecraft integration, and the number of interfaces required, thereby reducing the number of interconnects for the feeds and their associated electronics.

The antenna feed system assumed for the MSS is a non-overlapping feed design. It has been shown that with the 7-band frequency reuse arrangement, it is possible to achieve better than 22 dB carrier-to-cochannel interference isolation (C/I) in the coverage region using simple feeds composed of 4 microstrip patches each. This relatively simple feed array/beam forming network has the advantage of smaller size and lighter weight, compared with a more complex feed system with lower sidelobe performance. The achievable gain for this non-overlapping array is about 1 dB below the nominal optimum value. Although other types of feed elements can be used, microstrip patch feed elements are selected due to their simplicity, light weight, ease of implementation and the fact that they lend themselves quite naturally to an integrated flat and compact feed array design. The feed dimensions and array shapes can be seen in Figure 6-2 and 6-3.

FIGURE 6-1. LMSS ANTENNA GEOMETRY

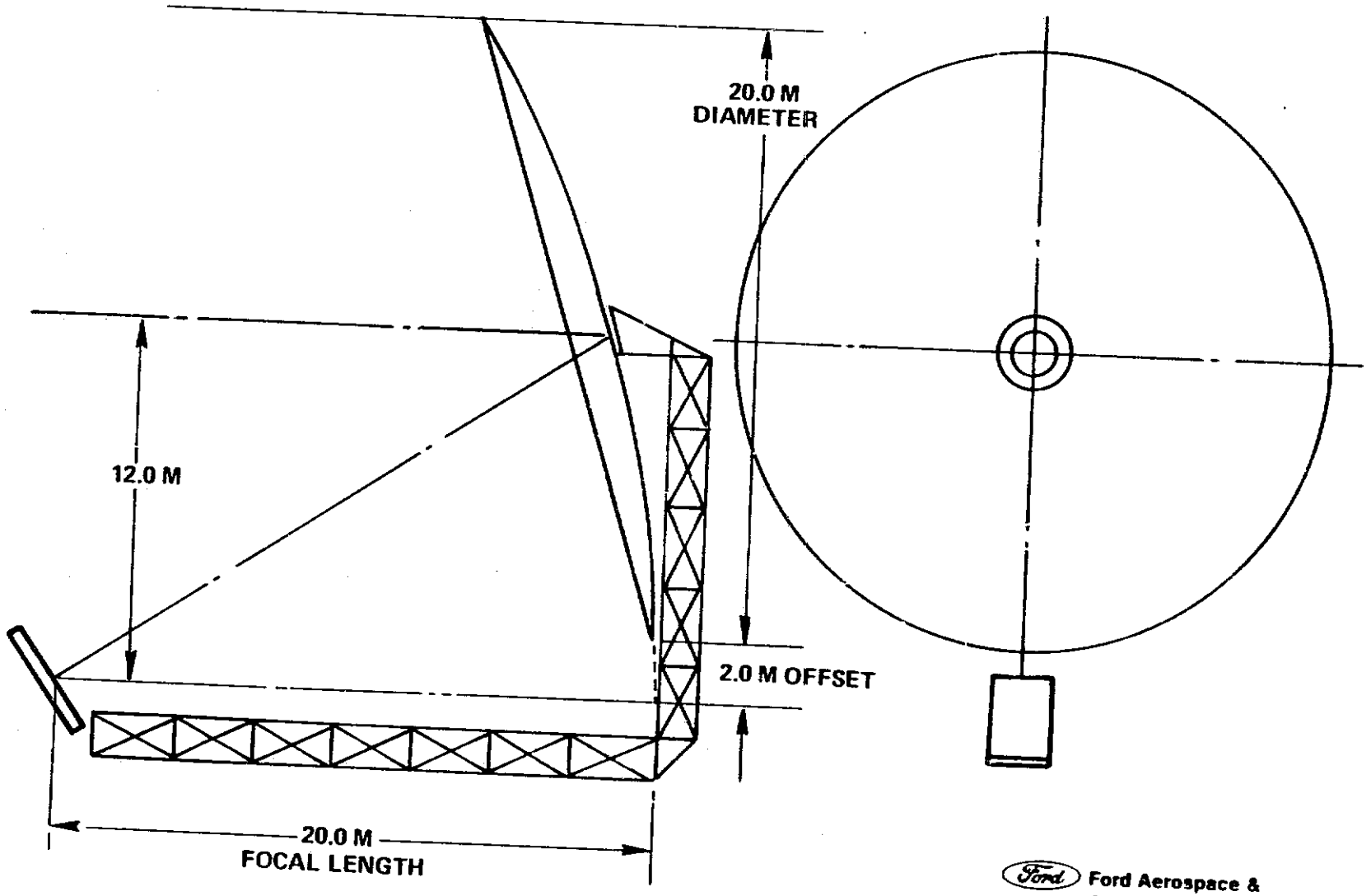

Ford Aerospace &
Communications Corporation

FIGURE 6-2. FEED ARRAY CONFIGURATION FOR MSAT-2 20m REFLECTOR ANTENNA: 130° LONGITUDE, 21 BEAM COVERAGE.

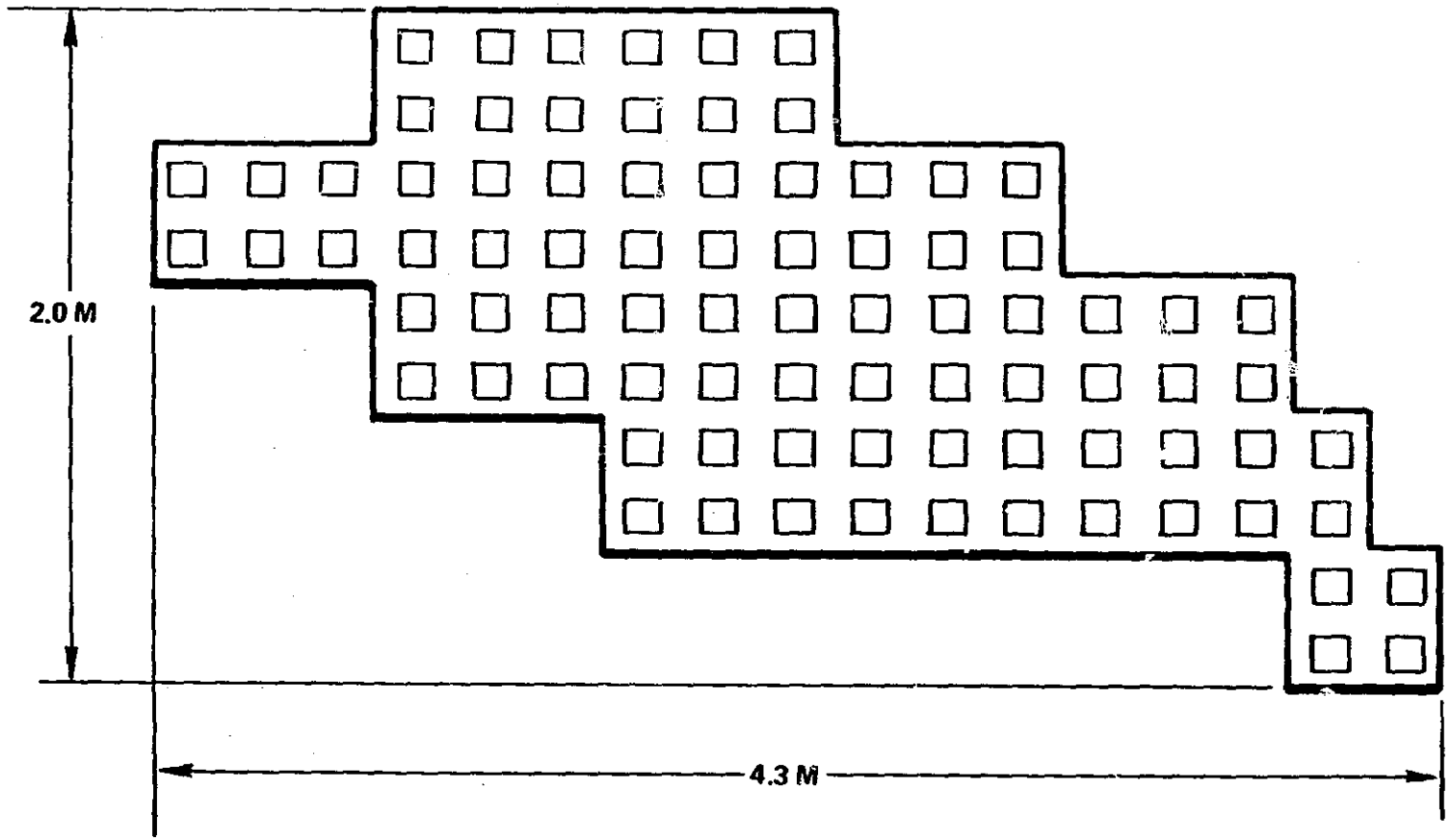

Ford Aerospace & Communications Corporation

FIGURE 6-3. FEED ARRAY CONFIGURATION FOR MSAT-2 20m REFLECTOR ANTENNA: 90° W. LONGITUDE, 24 BEAM COVERAGE.

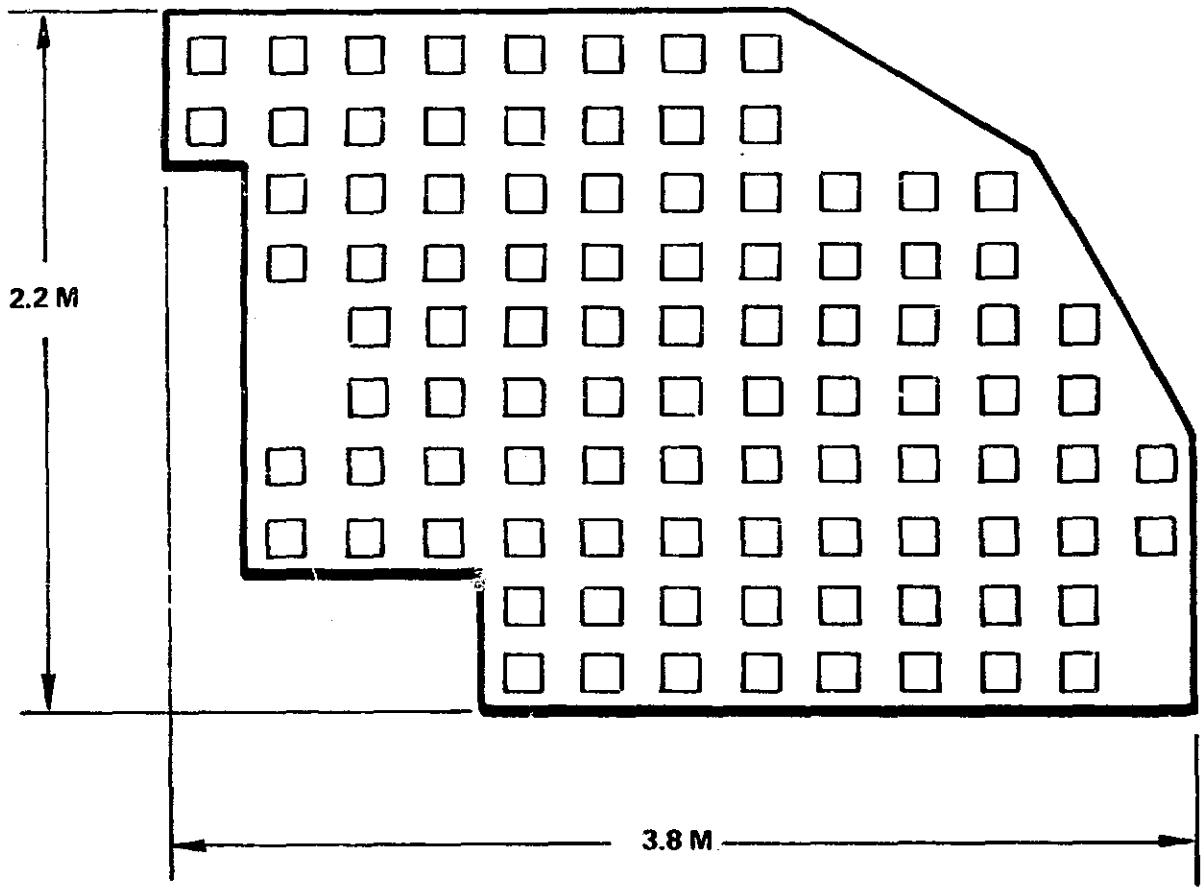

6.2 Multipacting Effects - Interconnect Cabling

The recommended interconnect for the antenna feed is flexible cable, since the spacecraft configuration would require on-orbit feed deployment. Flexible cable is very well suited for this application and is flight qualified by use on multiple space programs. Further, studies by JPL on the application and use of flexible cables is well documented in NASA "technical report 32-1500" titled "Report on RF Voltage Breakdown in Coaxial Transmission Lines" by R. Woo. This document shows that the flexible cable is acceptable in this frequency range. However, the transitions from cable to connector must take into account the fd (frequency-distance) characteristics to prevent multipacting at the cable/connector interface. The cable/connector multipacting is a solvable problem by using dielectric to fill the transition area and testing to verify the workmanship. Since the antenna is planned as a dual frequency transmit and receive system PIMS (passive intermodulation products) must be given serious consideration at this frequency and power. Due to limitations of time and allocation PIMS and their associated solutions are beyond the scope of this study and are only listed because of the potential problems that can result if PIMS are present.

6.3 Feed Deployment Mechanism

The concept for UHF feed deployment is shown in Figure 6-4. This design is a modification of existing mechanisms used on multiple spacecraft programs and is considered flight qualified. The design is a machined aluminum truss-like structure, which provides the structure/feed mounting interface and incorporates the spring deployment energy for the feed. The

FIGURE 6-4. UHF FEED DEPLOYMENT

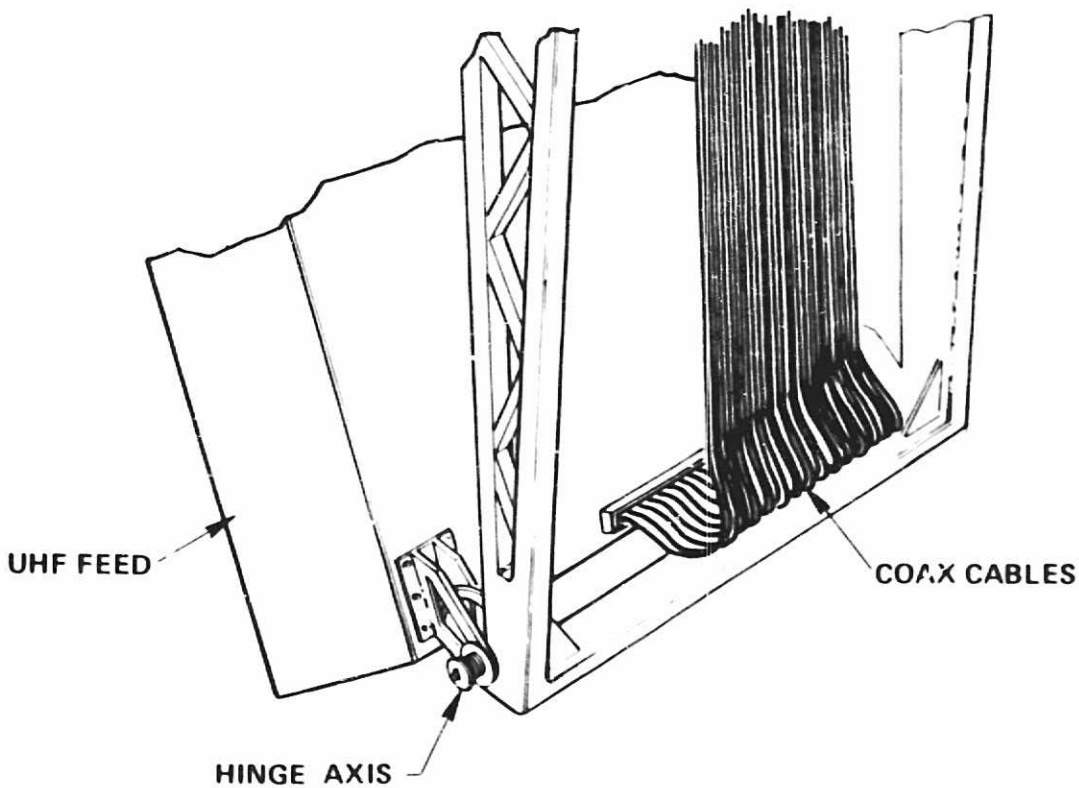

mechanism design provides a cam-follower to guide the feed deployment and a latch for positioning lockup. The aluminum structure is light-weight and rigid for launch and latch-up loads.

6.4 Passive Intermodulation

If the spacecraft resource constraints (power, mass and physical size) limits our selection of the antenna to a single antenna for both transmit and receive, then attention in the design of the antenna (both feed and reflector) should be paid to avoid passive intermodulation.

Pass Intermodulation (PIM) is a non-linear interference phenomenon caused by passive devices, much like the intermodulation interference generated by a non-linear, active devices, such as the TWTA, in multiple carrier operation. Passive IM has been identified as a serious threat to multicarrier communications systems. Particularly, in high power systems with low noise receivers, surprisingly high levels of PIM can be encountered and can seriously degrade system performance. In the high power transmit side, presumably linear components such as coaxial cable connectors or discontinuities in antennas or reflector panels, can behave non-linearily and generate intermodulation products with frequency in the receive band. With a sensitive receiver, these PIM products can be very harmful for the received, wanted signals.

Detailed investigation of passive component IM generation at Ford Aerospace was begun in 1972 following isolation of the PIM generation in the USASCA HT-MT antenna development. Most recently, a detailed investigation, on

passive intermodulation has been conducted in the INTELSAT V Maritime Communication System, an L-Band system.

Figure 6-5 shows the simplified block diagram of the I-V Maritime payload. It was found that when two signals were transmitted from the L-Band transmitter, strong intermodulation products (7th and 27th products) were found at the L/C receiver (point A in the diagram). With a nominal signal level of 0 dBm, a PIM of about -20 dBm would cause the C/I to degrade to about 20 dB at point A which was unacceptable for the system.

The set of photos in Figure 6-6 represents the PIM products at point A before and after the PIM problem was cured.

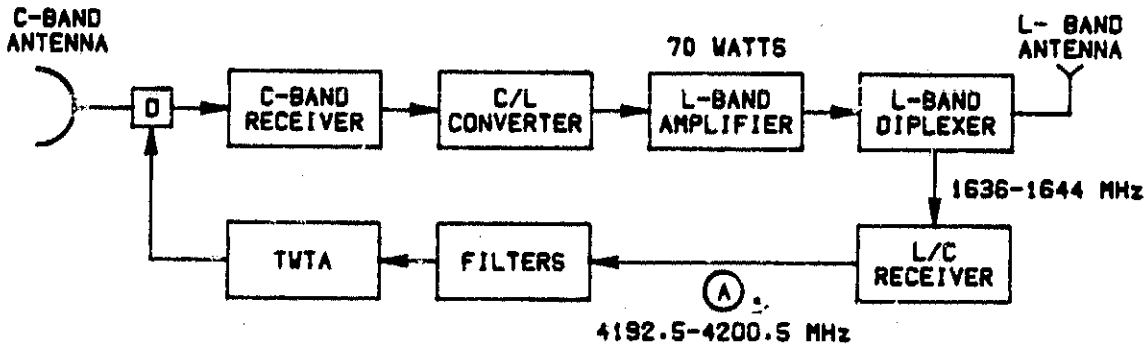

500274
KE650027/GAIL
1-18-84/MI

FIGURE 6-5 SIMPLIFIED BLOCK DIAGRAM OF INTELSAT V MARITIME TRANSPONDER

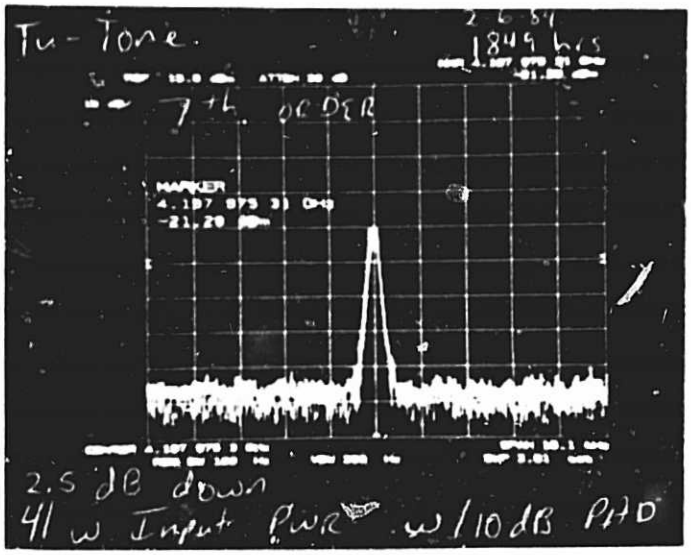

(A) 7th ORDER PIM

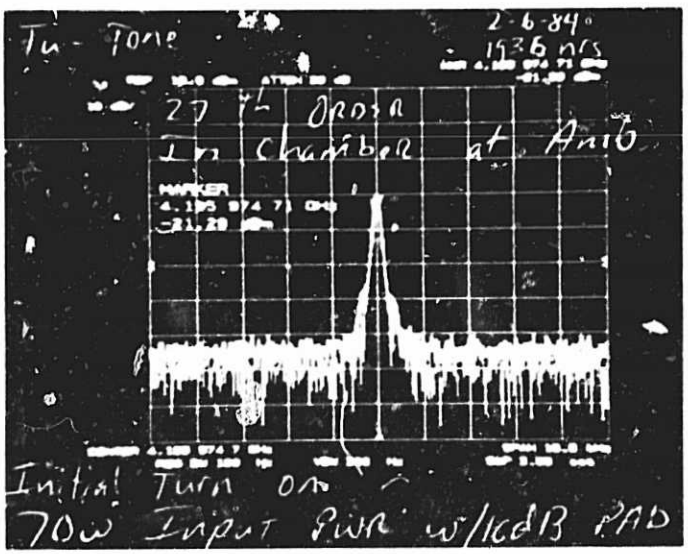

(B) 27th ORDER PIM

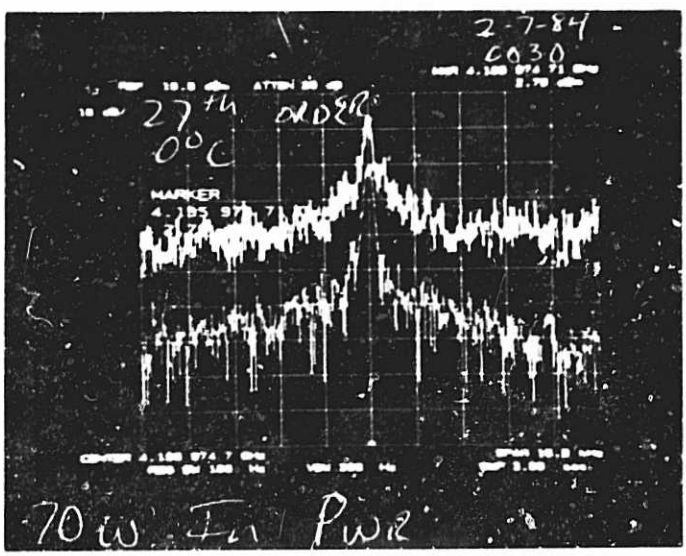

(C) 27th ORDER PIM AND NOISE FLOOR RAISED BY PASSIVE INTERMODULATION EFFECTS

FIGURE 6.6 SPECTRUM OF PASSIVE INTERMODULATION PRODUCTS (BEFORE THE PIM PROBLEM WAS CURED)

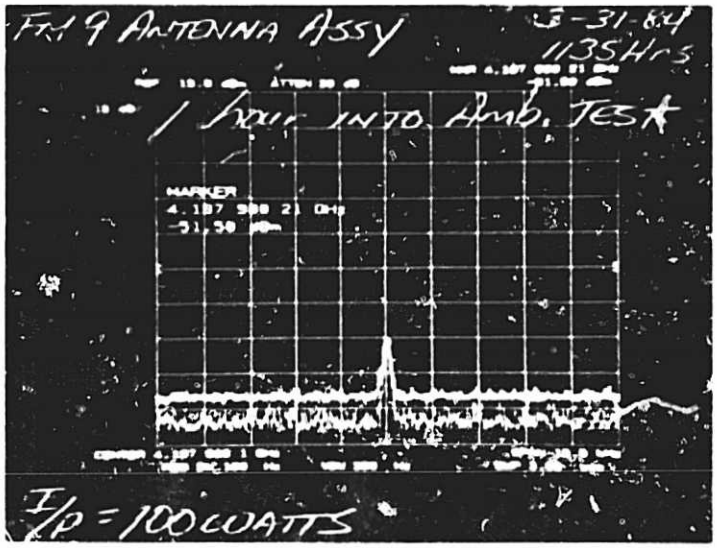

(E) 7th ORDER PIM

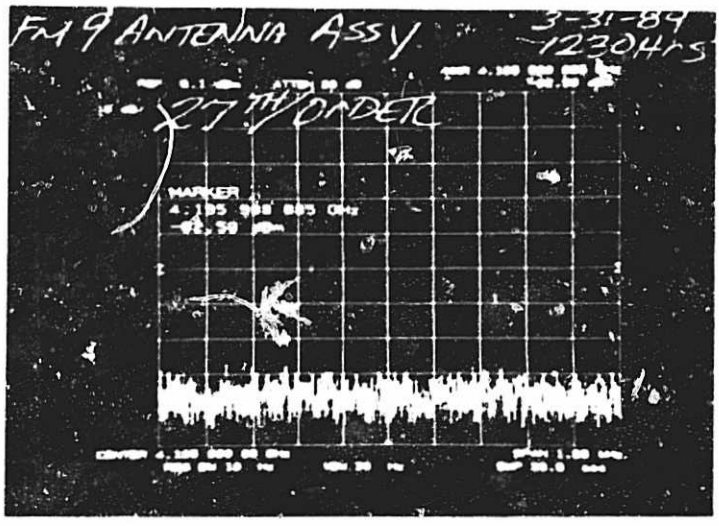

(F) 27th ORDER PIM

FIGURE 6.6 (Cont.) SPECTRUM OF PASSIVE INTERMODULATION PRODUCTS
(AFTER THE PIM PROBLEM WAS CURED)

After detailed investigation and antenna modifications, the PIM problem has been cured. Photos (E) and (F) in Figure 6.6 represent the controlled PIM products at point A after the problem has been resolved.

The current research has identified several potential causes of PIM within any communications system.

1. The presence of ferromagnetic materials in the system hardware such as connectors causes serious problems. The mere presence of large amounts of ferromagnetic materials in nearby structures such as antennas can cause PIM phenomena. This is probably not surprising because the ferromagnetic phenomenon is by its very nature non-linear.

2. The existence of Metal-Insulator-Metal (MIM) junctions which are exposed to the carrier frequencies can result in non-linear behavior which can in turn result in PIM generation. These junctions are usually found to be caused by naturally occurring oxides which are present on the metals used in the system, but as mentioned in (4) can also result from poor workmanship.

3. Microdischarges can be caused by microcracks, whiskers and voids in metal structures, and these can cause PIM generation.

4. Workmanship has also been found to be a cause of PIM; not directly of course, but loose connections or the existence of dirt in connections can create microdischarges or MIM junctions which in turn create PIM interference.

5. Finally, all materials are at some level non-linear, and even non-ferromagnetic materials will exhibit PIM phenomena albeit at a very low level.

Research has identified most of the potential causes of PIM but it has been less successful in finding cures for the problem. A number of guidelines have been proposed which will help mitigate the PIM problem but it is not possible to apply all of them in any particular situation.

1. Appropriate choice of frequencies to avoid overlap with interference.

2. Adequate separation of Transmission and Reception equipment to avoid generation of PIM's.

3. Appropriate choice of materials for the system components, the banning of all ferromagnetic materials in particular.

4. Careful attention to workmanship.

These primary rules should be used for the MSS design, but even careful attention to all the guidelines will not guarantee that a system will be PIM free. Only adequate system testing in both the design and production stages will assure that a system will perform as required.

7.0 TRANSPONDER LINEARIZATION TECHNIQUES

7.1 Introduction and Summary

Existing and potential linearizers applicable to the Land Mobile Satellite user downlinks were surveyed and evaluated. The performance criteria used in evaluating the potential linearization techniques were:

- o DC/RF efficiency
- o Compatibility with the MSS channel parameters, ie, 880 MHz, 1.4 MHz bandwidth channels, 20-40 watts usable RF output power, SSB or low data rate digital (pm) modulation techniques, minimum 25 dB C/I.

Linearizer Survey

The following linearization techniques were surveyed.

- o Brute force (output RF backoff)
- o Improved EER with envelope feedback
- o Feed forward (post distortion)
- o Predistortion
- o RF (cavity) feedback

Figure 7.1-1 summarizes the operational principles of these techniques. Sections 7.2 through 7.6 describe each linearization approach in detail.

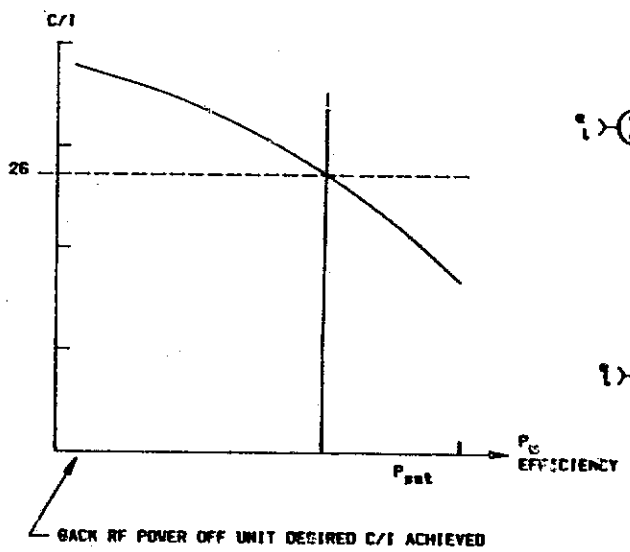

(A) BRUTE FORCE (RF BACKOFF)

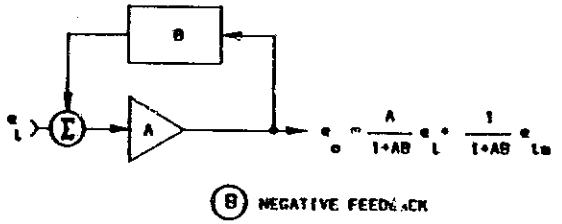

(B) NEGATIVE FEEDBACK

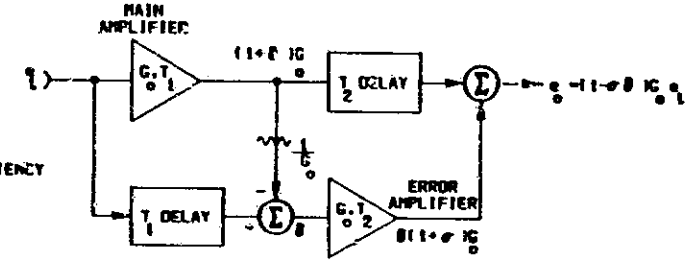

(C) FEEDFORWARD

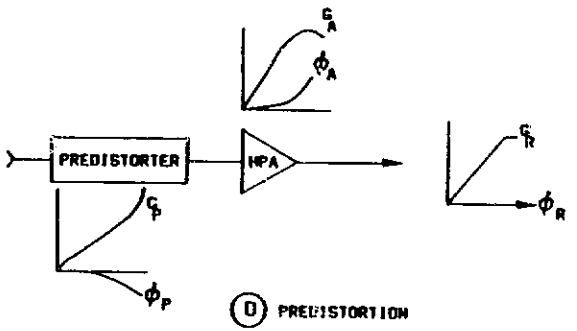

(D) PREDISTORTION

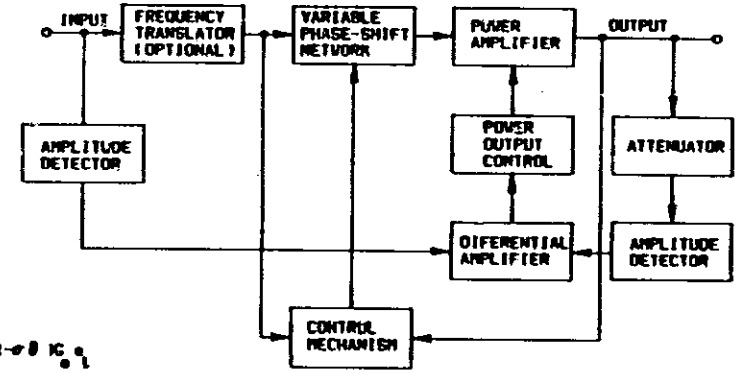

(E) ENVELOPE FEED BACK (INPROVED EER)

FIGURE 7.1-1 SUMMARY OF TRANSPONDER LINEARIZATION TECHNIQUES

Linearizer Evaluation

The five potential linearization techniques were evaluated in relative terms for air efficiency, complexity, and development risk. Table 7.1-1 summarizes this evaluation.

Table 7.1-1 Comparison of Linearization Techniques

Linearization Technique	Relative Efficiency	Relative Mass(1,2)	Relative Complexity	Relative Devel. Effort
Brute Force (RF output backoff)	4 (22-26%)	1 (1.0)	1	1
Improved EER (Envelope Feedback)	1 (33-50%)	4 (1.4)	5	5
Cavity RF Feedback	2 (28-34%)	2 (1.1)	2	2
Predistortion	3 (28-33%)	3 (1.2)	3	3
Feed Forward (Post distortion)	5 (15-20%)	5 (1.7)	4	4

Notes:

(1) PA + linearizer mass; does not include weight of solar panels, batteries, thermal, etc associated with efficiency ratings.

(2) Numbers in parenthesis are estimated ratios (relative to brute force mass)

All linearization techniques except feed forward are potentially useful for the Land Mobile Satellite user downlinks. The feed forward technique is judged to be inappropriate for MSS since its potential linearization improvements are negated by its need for a second amplifier with attendant mass and power.

The brute force was used for the yardstick in this evaluation. This approach is the simplest, requiring no additional linearizer circuitry, and has the minimum development risk. The required 26 dB C/I could be obtained with an estimated 24% DC/RF efficiency using the brute force backoff approach. Depending upon the spacecraft bus chosen and its primary power capabilities, the brute force approach may well be adequate for the second generation MSS mission.

The improved EER approach, with envelope feedback, offers the highest potential overall efficiency (33-50%). It is by far the most complex approach, however, and requires further analysis to verify its feasibility for handling angle modulation and for operation over a 1.4 MHz channel bandwidth. A large development effort would be required to achieve a flight qualified EER unit.

For somewhat less efficiency improvement and much less development, the RF (cavity) feedback approach appears promising. Predistortion would yield approximately same efficiency as cavity feedback, and have less bandwidth restrictions, but requires considerable additional circuitry plus extensive integration time to tailor each predistorter to its associated PA.

Recommendation for future efforts:

The following future efforts are recommended to provide the basis for selecting an MSS linearization approach:

1. Quantitatively evaluate capabilities of cavity feedback - breadboard amplifier at nominal frequency, bandwidth, output power, evaluate performance vs cavity bandwidth, amount of feedback employed, at nominal and max output power levels. Determine performance under conditions of many input signals - determine if pre-clipping is necessary or desirable. Compare performance against brute force performance.

2. Replace cavity feedback with predistorter and repeat tests. Compare predistorter and cavity feedback performance.

3. Analytically evaluate the improved EER approach in sufficient detail to verify its feasibility and potential efficiency improvements for MSS. Specifically,

   - o Model the feedback loops and time delays to assure the required bandwidth can be achieved.

   - o Analyze the high-speed switching regulator requirements to verify that a high-efficiency regulator can be achieved at the MHz rates required.

   - o Analyze the performance with angle modulated signals to determine. if the required C/I performance is attainable with FM or PM modulation.

7.2 Brute Force Approach (Backoff)

7.2.1 Operation

In terms of RF hardware complexity, the simplest approach to achieve the MSS linearity requirements is to use a class AB/B amplifier backed off from saturation. No other linearization techniques are used; the required linearity is achieved at the expense of efficiency and resulting spacecraft power.

This brute force technique provides the yardstick by which the effectiveness of other linearization techniques can be measured. If spacecraft primary power is not a limiting factor, brute force must also be considered as a serious candidate due to its relative simplicity and low development risk.

To assess the DC/RF efficiency of the brute force approach, one must establish the criteria for acceptable linearity. For the second generation Land Mobile Satellite, the following requirements are assumed:

Frequency	880 MHz
Bandwidth	1.4 Mhz
Average Po	12-20 watts
Max Po	3 dB above average
C/3IM	26 dBc (2-tones, equal power)

7.2.2 Performance

FACC has developed and flown a 70-watt 1550 MHz quasi-linear transmitter for the Intelsat V Maritime Communications Subsystem (MCS). This high power transmitter is designed to accommodate SCPC operations with low intermodulation distortion and is sufficiently close to the MSS requirements to use as a basis for performance predictions. Key performance parameters are:

Frequency	1540 MHz
RF output power, min	
High power	48.3 dBm (67.6 watts)
Low power	45.3 dBm (34 watts)
Bandwidth	7.5 MHz minimum

Passband flatness	0.15 dB
Gain	65 dB
Overdrive	20 dB (no damage)
Phase shift	46 deg max
AM-PM transfer	10 deg/dB max
C/IM	12 dB (max input level, noise power loading)
DC power, max	
High power	247 W
Low Power	132 watts
Operating Temp.	-10 to +61 deg C

The block diagram of the MCS transmitter is shown in Figure 7.2-1. It consists of an input limiter/amplifier, driver output, two 40-watt power amplifiers, and DC/DC converter. It can be operated in the low power (40-watt) mode using either amplifier. When the high power mode is selected, both amplifiers are operated in parallel with their outputs combined in a hybrid. In the low power mode the selected amplifier is connected directly to the output port.

The input limiter is a peak clipper used to protect the amplifier under overdrive conditions.

It should be noted, in using the MCS performance to predict the performance of a brute force MSS transponder, that the MCS transmitter's performance is specified in terms of AM/PM conversion, phase shift vs drive, and noise power loading (NPR) performance - two-tone C/3IM is not a specific requirement and was not necessarily optimized in the design or alignment. The MCS transmitter C/I performance is therefore somewhat pessimistic compared to what could be achieved for an MSS transmitter design optimized for C/3IM performance.

Figure 7.2-2 presents the C/3IM performance and DC/RF efficiency vs output backoff from nominal RF drive for a typical MCS transmitter flight unit. Performance is given for each of the two 40-watt power amplifier sides.

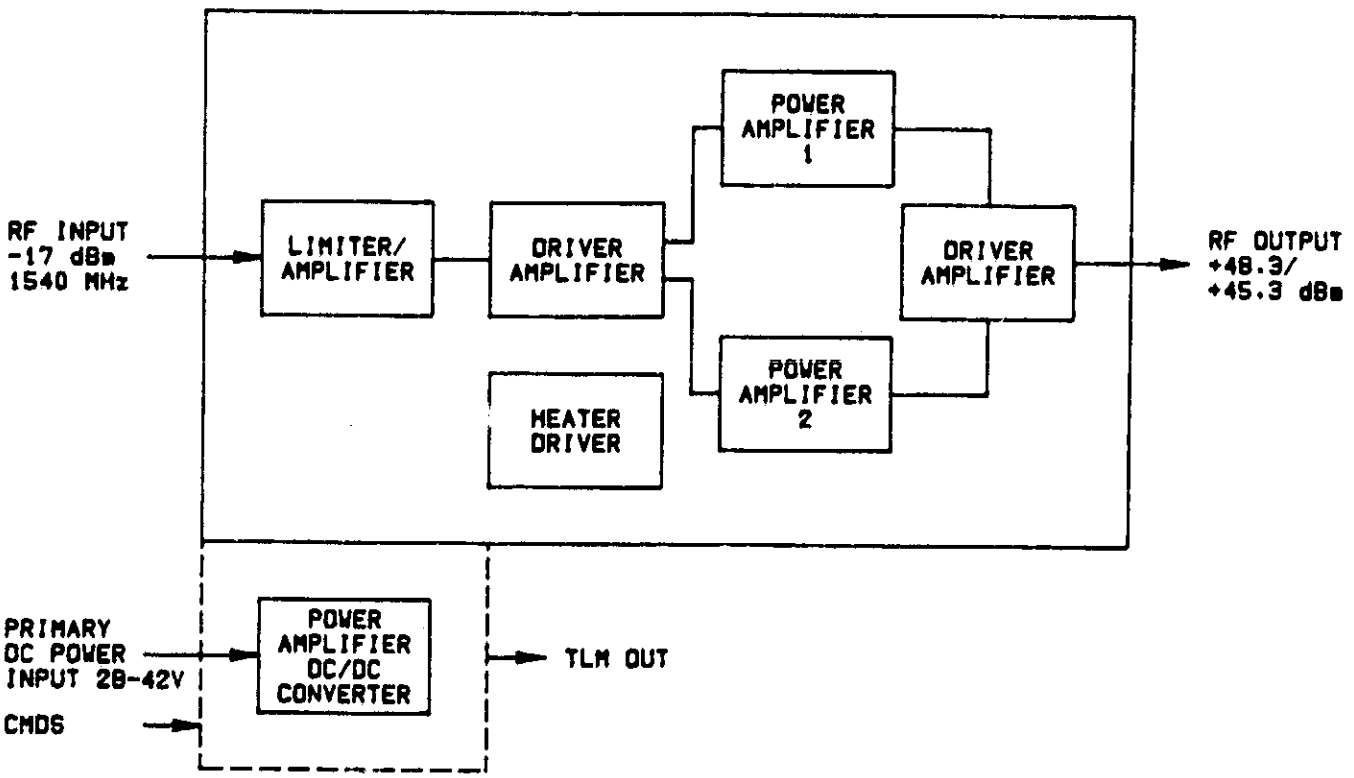

500275

KEL50039/GAIL1
1-23-85/GM/MISC1

FIGURE 7.2-1 INTELSAT-V MCS PA BLOCK DIAGRAM

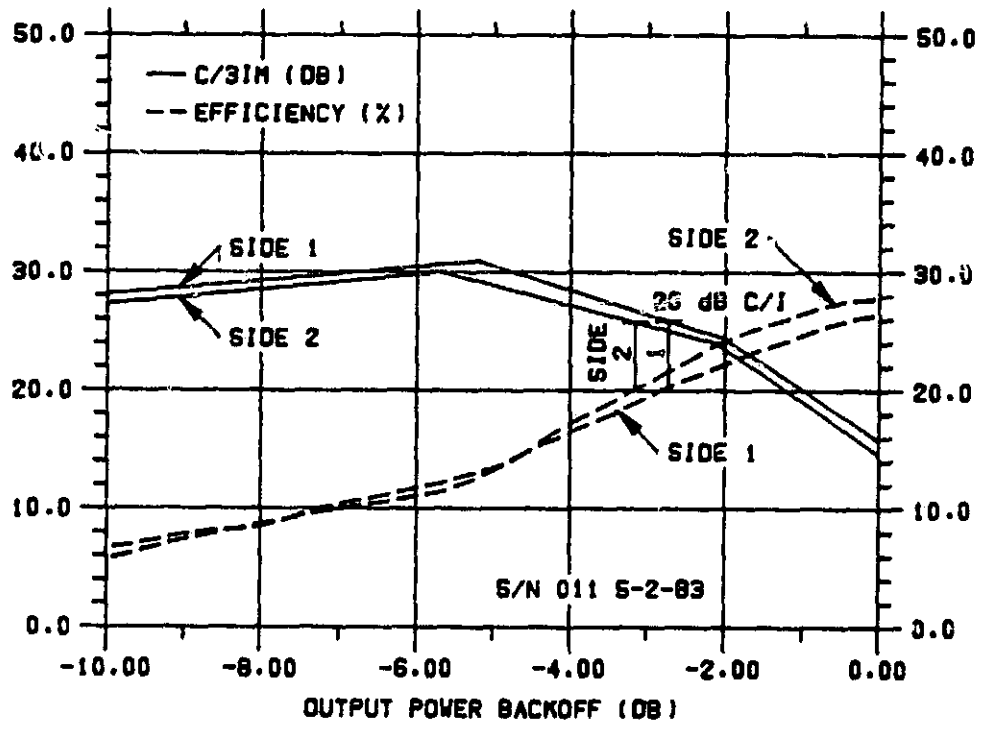

500276
KE650027/GAIL
1-18-85/M1

FIGURE 7.2-2 MARITIME L-BAND POWER AMPLIFIER C/3IM & EFFICIENCY

It should be pointed out that for the MCS design, the nominal drive is slightly (approx 0.5 dB) below the single-carrier saturation level.

At nominal drive, the C/3IM performance is 15 to 15.5 dB and efficiency is 26 to 28%. C/3IM performance of 26 dB is achieved for both amplifiers at a nominal 3 dB output backoff with corresponding operating efficiencies of 20%. This data was taken at room temperature and nominal bus voltage. A minimum 18% worst-case efficiency is estimated over temperature, bus voltage variations, and life.

The MCS amplifier design uses 4 parallel transistors, each having a stage efficiency of nominally 50% at 0 dB backoff. It is estimated that a similar, 1990 time frame design for a 40-watt, 880 MHz PA could be achieved with two paralleled output stages, with each stage having a 0 dB backoff efficiency of 65%. With the elimination of one output combiner (0.15 dB improvement) and increased stage efficiency, an efficiency improvement factor of 1.35 would be realized.

Applying this 1.35 improvement factor to the 18% worst-case MCS performance, an estimated 24% Land Mobile Satellite PA efficiency could be obtained for a 26 dB C/3IM performance using the brute force backoff approach.

7.2.3 Advantages and Disadvantages

Brute force linearization achieves the required linearity by simply using a power amplifier having high saturation output level and backing off the drive (and RF output power) until the required linearity is achieved.

This approach is simple, reliable, and good for all modulation types. There are no bandwidth constraints.

Its key disadvantage is its relatively low efficiency compared to other linearization techniques.

7.3 Envelope Feedback (EER)

Modern envelope feedback techniques (e.g., OSCAR 7, Sokal's 1975 patent, HELAPS, etc.) are improvements upon L. Kahn's original 1952 envelope elimination and restoration (EER) method. Envelope feedback, when properly implemented, yields a highly efficient and linear system. Its implementation is quite complicated however, and the system requires careful balancing of components and control of parasitic influences.

7.3.1 Description of Operation

Figure 7.3-1 presents a simplified block diagram of an improved EER implementation.

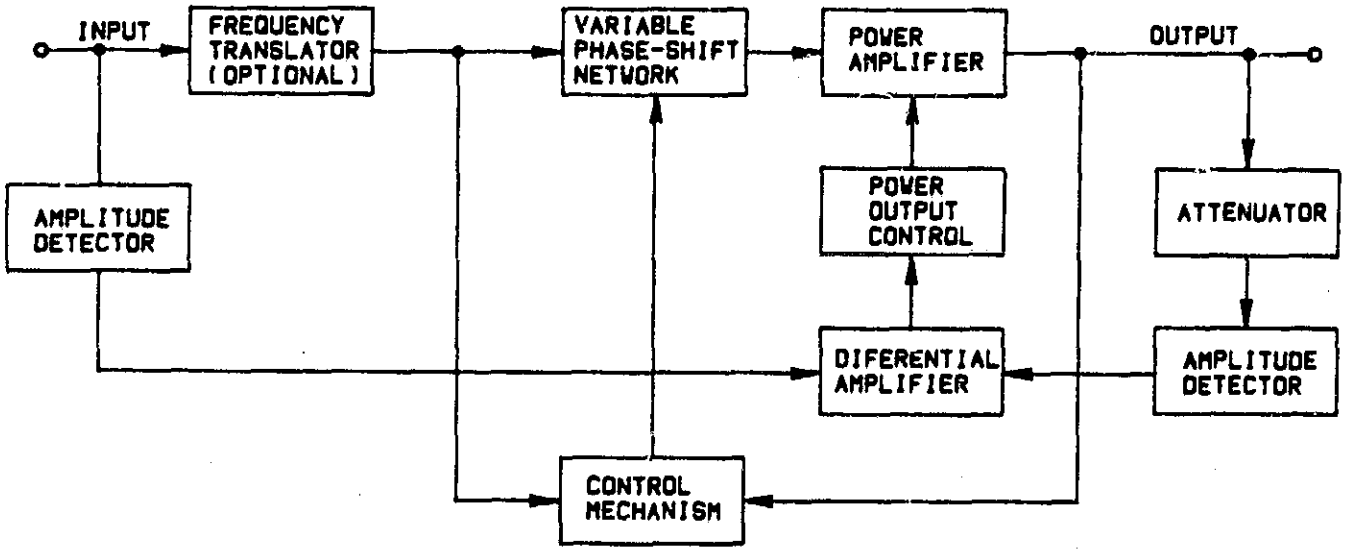

500390
KEL50039/GM1
1-23-85/GM/MISC1

FIGURE 7.3-1. IMPROVED EER AMPLIFIER BLOCK DIAGRAM

The basic approach is straightforward in theory. The input signal is split into two paths, amplitude and phase. The phase path is hard-limited to remove the amplitude information and drives a high-efficiency CW amplifier. The amplitude path is envelope detected to recover the amplitude information.

A square wave signal operating at several times the highest frequency component of the AM envelope is pulse-width modulated by the AM signal. the PWM signal controls a fast-switching regulator. The regulator output is filtered to recover the AM signal and then modulates the collector voltage of the CW amplifier, resulting in an amplified reconstruction of the input signal. A sample of the amplifier output is AM detected. This signal is then used in a feedback loop to increase amplifier linearity. In more sophisticated systems, phase feedback is also provided.

This technique enables the amplifier to be of a high-efficiency switching type. Efficiency is maintained over the input dynamic range since the collector voltage is varied, not amplifier input drive.

7.3.2 Performance

An envelope feedback transponder (146 MHz transmit frequency, 50 kHz bandwidth) was built and flown on the OSCAR 7 amateur radio satellite. Efficiency and intermod performance are summarized below (ref. 2).

Sokal (ref. 3) has reported efficiencies of 85% and IM levels less than 40 dB achieved over a voice channel bandwidth at HF (3.9 MHz) using an improved EER system with a class E rf stage and a switching regulator modulator.

King (ref. 4) states that Skylink, using a proprietary HELAPS technique, can achieve an efficiency of 33-45% for high-power 800 MHz transponders with 30 dB C/I ratios.

Table 7.3-1. OSCAR 7 Efficiency and C/I Performance

Drive	Pout	Power Consumption	Efficiency	Intermodulation during two-tone test
0 dB	11.2 W	25.3 W	44%	3rd order - -34 dB
-3 dB	5.6 W	13.2 W	42%	5th order - -40 dB
-6 dB	3.0 W	7.5 W	40%	(referred to 11.2 W)
-10 dB	1.2 W	3.6 W	33%	

Advantages:

The improved EER approach offers extremely high efficiency compared to other linearization techniques. The technique is flight-proven in the 146 MHz band (OSCAR 7). Efficiencies of 30-50% at 800 MHz with C/I ratios of 30 dB are potentially available.

Disadvantages:

The approach is extremely complex, requiring:

- o high efficiency RF power amplifier design;
- o high efficiency switching regulator having a fast output response over the AM envelope bandwidth (2-3 times the channel bandwidth, or in excess of 3 MHz). This poses a challenging design problem;
- o critical matching of circuit elements, e.g., detectors;
- o careful control of parasitic elements (delay differences through amplitude and phase channels, phase lags in switching regulator, tracking of system responses over dynamic range, etc.).

In addition, most of the available data is for narrow-band AM and SSB systems. Further investigation is required to determine what performance could be achieved for angle-modulated signals or for the 1.4 MHz wide MSS channels.

7.4 Feedforward

Feedforward was first conceived by H.S. Black in 1924. Harold Seidel of Bell Laboratories investigated and experimentally verified its effectiveness in improving amplifier linearity starting in the late 60's (references 5,6). The feedforward technique does not use feedback, so RF transit time delays are not important, and amplifiers with long transit times, e.g., TWTAs, can be effectively linearized over wide bandwidths. The feedforward approach, however, requires two amplifiers instead of one, in addition to couplers and delay lines with tight requirements, so it is relatively unattractive for space applications.

7.4.1 Description of Operation

Figure 7.4-1 presents a simplified block diagram of a single-stage feedforward control system. The input signal is split into two paths. One path drives the main amplifier. A sample of the amplifier output, at a level of 1/G, where G is the main amplifier gain, is fed to one input of a comparator. The other input to the comparator is the input signal (from the other output of the input splitter), which has been delayed by a factor, T1, equal to the time delay of the main amplifier.

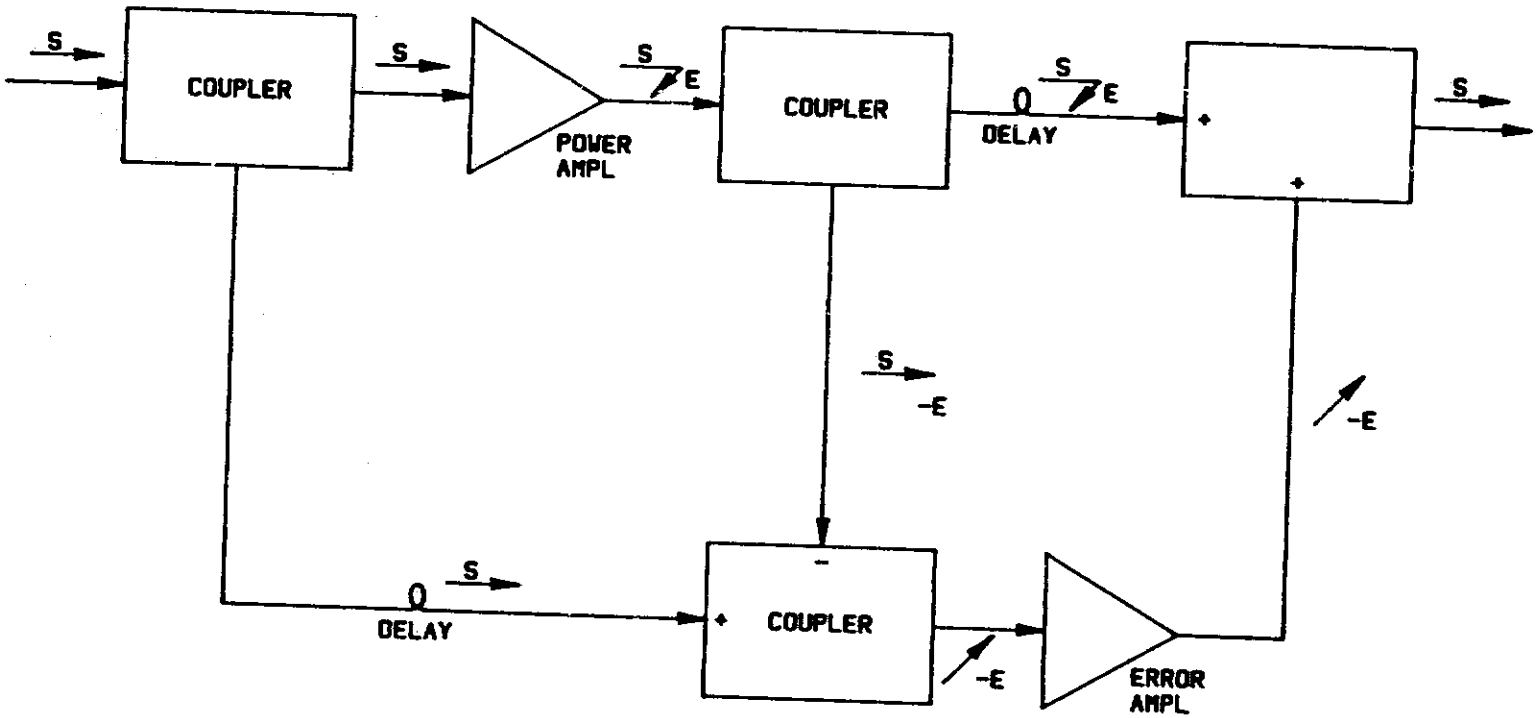

855052

KEL50039/JE1
1-23-85/GM/MISC1

FIGURE 7.4-1. FEED FORWARD LINEARIZED AMPLIFIER

Any non-linearity (amplitude or phase) introduced by the main amplifier is output by the comparator as an error signal. This error signal is then routed through the auxiliary (error) amplifier. The auxiliary amplifier has the same gain as the main amplifier. Thus, its output is an error signal equal in magnitude and phase to that of the distortion in the main amplifier output. (Since this auxiliary amplifier is only handling the error signal, it is operating in a linear mode and introduces only very small errors due to its nonlinearities.)

The output from the auxiliary amplifier is then subtracted from the main signal in an output coupler. A second time delay, T2, is introduced between the main amplifier output and this coupler to compensate for the time delay of the auxiliary amplifier.

The resultant output signal has only residual low-level error (distortion) products due to the nonlinearity of the auxiliary amplifier and the unbalances of the system couplers.

7.4.3 Performance

Seidel has demonstrated 3IM reductions for a 20 MHz bandwidth, 4 GHz TWTA amplifier of over 38 dB using feedforward linearization. These results were time independent over several months, demonstrating the inherent long-term stability of the feedforward technique (6). However, his experiments were performed on an amplifier already working in a very linear mode, so it is unclear how this directly applies to increased DC/RF efficiency for a given C/I performance.

ELAB of Norway has performed experiments with similar feedforward techniques on a 4 GHz TWT amplifier for satellite communications. Bakken (7) shows data indicating that a feedforward TWT amplifier can be operated 4 dB closer to saturation relative to a single TWTA and achieve 26 dB C/I performance. Again, however, it is difficult to determine from his paper the relative DC/RF efficiency of a feedforward configuration compared to a single amplifier.

7.4.4 Advantages and Disadvantages

The feedforward approach involves no closed loops, so it is unconditionally stable. Since feedback is not used, amplifier time delays are unimportant, and the approach can be used with devices such as TWTs over wide bandwidths. Although an additional amplifier is involved, the implementation is relatively simple.

The key disadvantage is that an additional amplifier, of essentially the same performance as the main amplifier, is required. This additional amplifier, with its attendant mass and power, makes the feedforward approach relatively unattractive for space applications.

7.5 Predistortion

Linearization by predistortion introduces a nonlinear distortion into the power amplifier input signal path. This predistortion is complementary in phase and amplitude to the PA's nonlinearity, yielding an overall transfer function with improved linearity.

Considerable study and experimentation has been performed in recent years toward the use of predistortion linearizers for broadband satellite power amplifiers [7-12] and ground-based SSB microwave amplifiers [13-14]. This high level of interest in the predistortion linearization approach stems from the following:

- o No feedback loops are involved, so significant linearity improvement is possible over wide bandwidths.
- o The predistortion approach enables use of existing PA designs (primarily TWTAs in current satellite designs, although FET SSPAs are becoming more commonplace), so relatively low development risk is involved in adding a predistortion linearizer.

7.5.1 Description of Operation

Overall design approach

The steps followed in linearizing a PA using predistortion are typically as follows:

First, the nonlinearities of the power amplifier are characterized. This characterization is typically based on the amplitude and phase characteristics of the PA vs drive. Figure 7.5-1(a) illustrates the typical amplitude and phase characteristics vs drive of a microwave TWTA amplifier. As the input drive approaches saturation, the gain is compressed and the phase shift increases.

Next, a predistortion network is synthesized which introduces a complementary nonlinearity to the input signal, ie, an expanding gain and decreasing phase shift (phase lead), as shown in Figure 7.5-1(b).

The predistortion network and PA are then integrated. The predistorter is aligned and compensated, including temperature compensation, to maximize the overall transfer linearity (specifically, to minimize the output backoff required to achieve the required C/3IM ratio). Figure 7.5-1(c) and 7.5-1(d) illustrate the resulting overall amplitude, phase, and C/3IM characteristics.

Predistortion network

The predistortion network (see Figure 7.5-2a) consists of the following elements: Input power splitter, a linear arm containing a time delay element (phase shifter) and attenuator, a non-linear arm containing the distortion generator, and an output hybrid combiner. Other components may include temperature compensation networks, an output amplifier to make up the loss through the network, a soft limiter (primarily used with TWT amplifiers to control overdrive), and PA phase/amplitude equalizers.

The typical network functions as follows:

The nonlinear arm contains a distortion generator. This may consist of a Shottky diode attenuator, FET attenuator, FET amplifier, bipolar amplifier, or other nonlinear circuit which simulates at low signal levels the amplitude and phase characteristics of the power amplifier to be linearized. The generator output is combined with the linear output in a hybrid combiner. The phase relationships of the two inputs to this combiner are such that the

FIGURE 7.5-1. PA LINEARIZATION CHARACTERISTICS

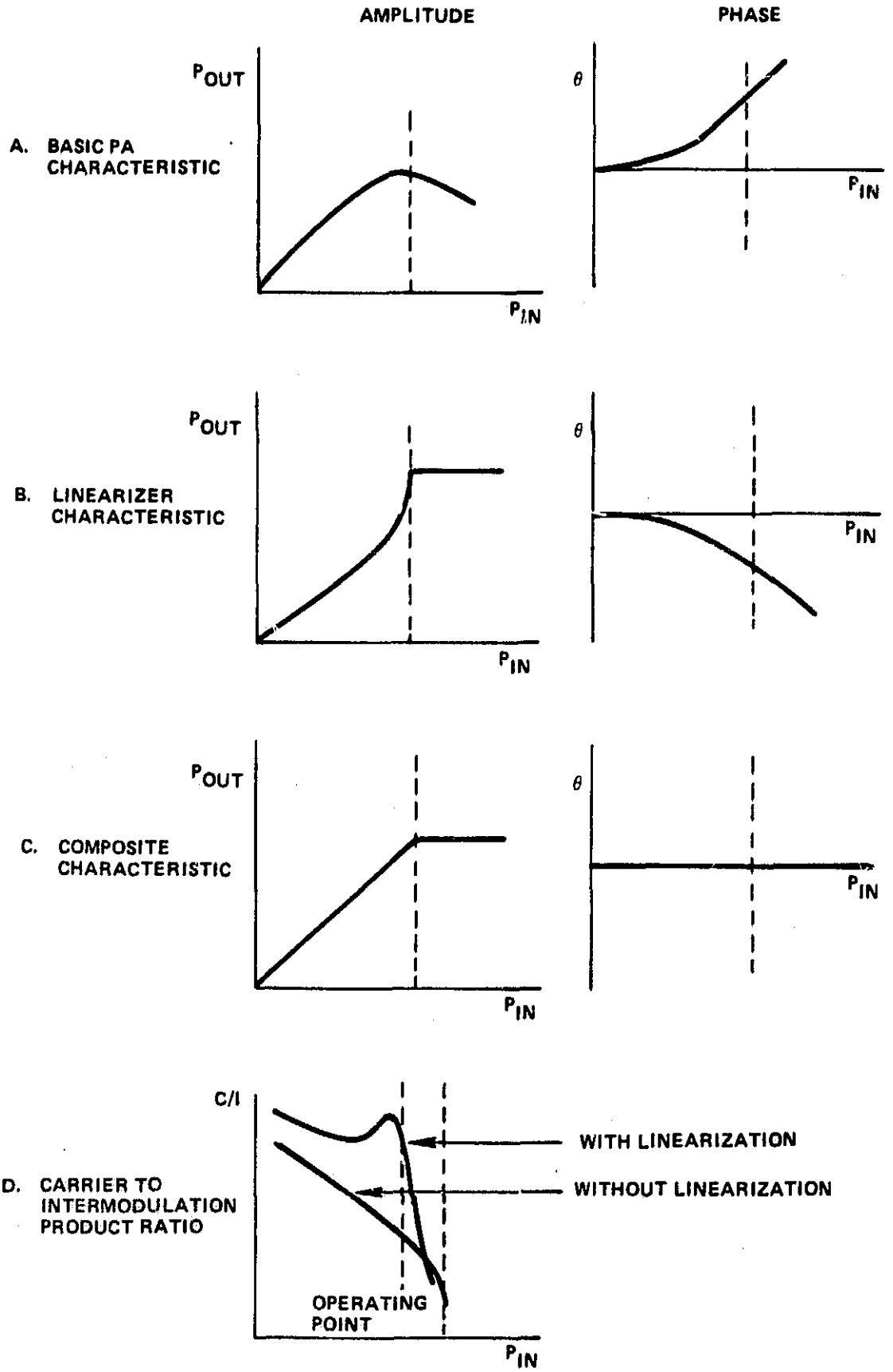

resulting output has the desired inverse characteristics of the power amplifier (refer to Figures 7.5-2b and 7.5-2c).

The other components which may be used (eg, output amplifier, limiter, equalizers) depend upon the channel requirements and type of amplifier being equalized. For the MSS application (relatively narrow bandwidth, solid- state power amplifier), these would probably not be needed.

7.5.2 Performance

Most of the available performance data relates to C or Ku-band satellite PAs, so the absolute efficiencies achieved are not directly applicable to the MSS. However, the improvement achieved in terms of how closely the PAs could be operated to saturation and still achieve high C/I ratios is relevant.

Figure 7.5-3 presents the results obtained by ANT-Germany using a 4 GHz FET PA with predistortion [11]. This work, performed for Intelsat, used a single stage FET amplifier as the linearizer. The figure compares the linearized FET PA with an unlinearized FET and a typical 4GHZ TWT amplifier. The linearized FET amplifier achieved C/I ratios in excess of 30 dB when operated at 3 dB output backoff. By comparison, the unlinearized FET required 6 dB output backoff to achieve similar performance, while the TWTA required 10 dB backoff. The DC/RF efficiency for the linearized FET amplifier was twice that for the unlinearized FET for a 30 dB C/I performance.

Other experimenters report similar improvements in C/I performance vs output backoff. Kumar and Whartenby of RCA [9] report a 30 dB C/I performance at 2.5 dB backoff of a 12 Ghz TWTA using a dual-gate MESFET attenuator as the

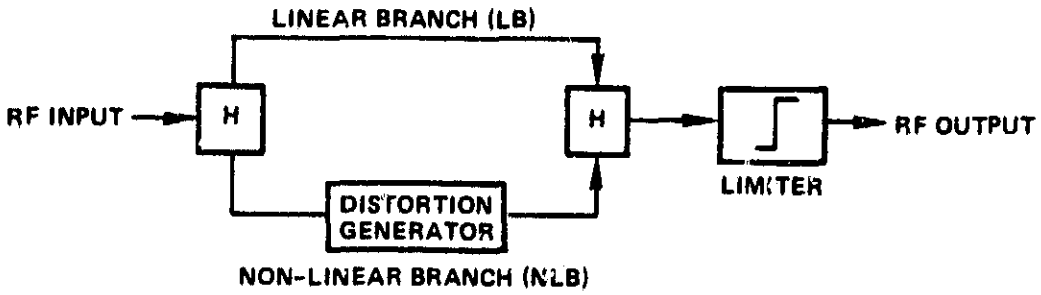

A) LINEARIZER CONCEPTUAL BLOCK DIAGRAM

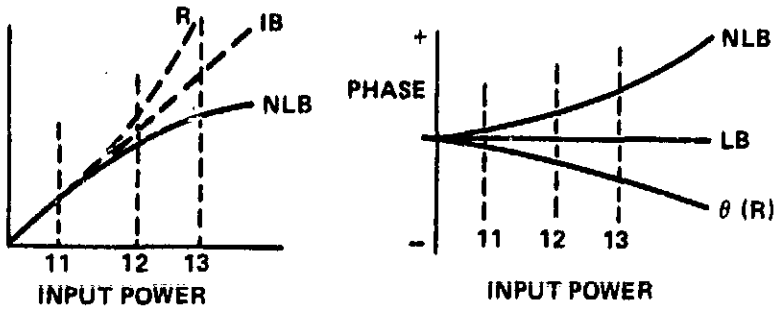

B) AMPLITUDE AND PHASE CHARACTERISTICS OF LINEAR AND NON-LINEAR BRANCHES

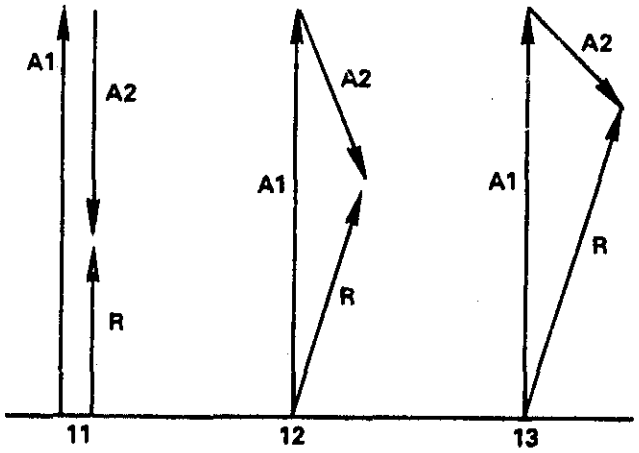

A1 = LB VECTOR A2 = NLB R = RESULTANT VECTOR

C) NORMALISED VECTOR DIAGRAMS SHOWING GAIN EXPANSION AND PHASE SHIFT FOR THREE INPUT POWERS

FIGURE 7.5-2. LINEARIZER DESIGN CONCEPT

REQUIRED IMR	P_{OUT}	OBO	P_{SAT}	η	P_{DC}	MASS
LIN FET PA						
20 dB	2.14 W	2.2 dB	3.5 W	20%	10.7 W	1.1 kg
30 dB	1.8 W	2.8 dB	3.5 W	16%	10.9 W	
FET PA						
20 dB	2.14 W	3.5 dB	4.8 W	15%	14.3 W	0.8 kg
30 dB	1.8 W	6 dB	7.2 W	8%	22.5 W	0.9 kg
20 dB	2.14 W	5.4 dB	7.9 W	13%	16.5 W	
30 dB	1.8 W	9.8 dB	16 W	6%	29.0 W	2.4 kg

A. MASS & POWER

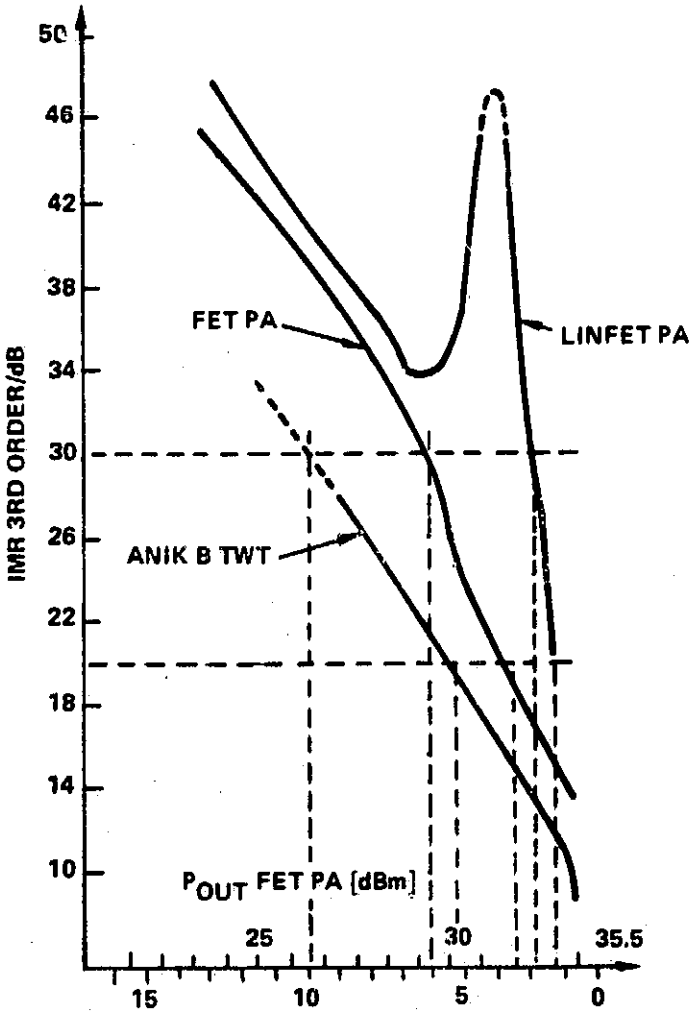

B. OUTPUT BACK OFF

TWO CARRIER 3RD ORDER IMR OF LIN-FETRA, FETPA, AND A TWT FROM ANIK B TYPE

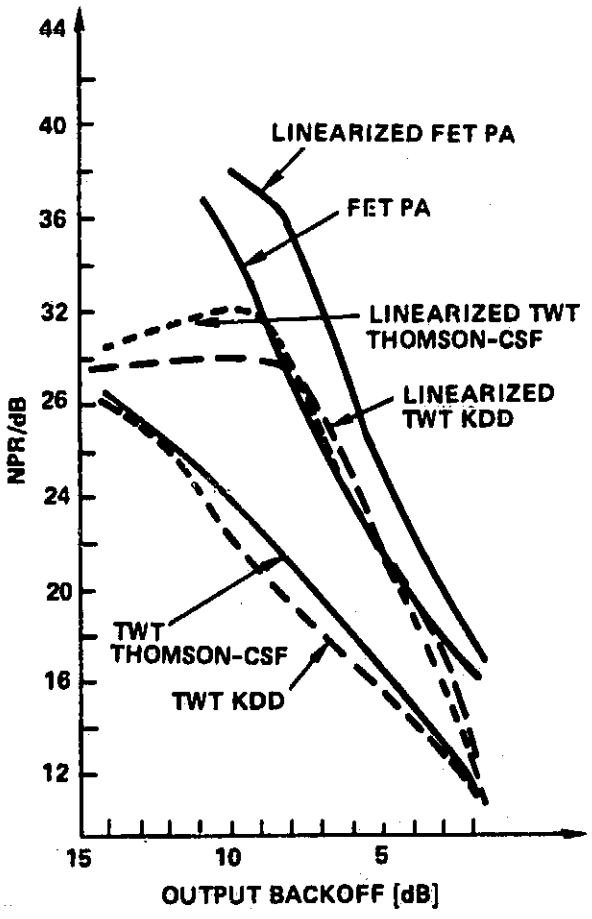

C. COMPARISON OF RESULTS OF NPR MEASUREMENTS

FIGURE 7.5-3. PERFORMANCE COMPARISONS FOR 4 GHz LINEARIZED SSPA VS UNLINEARIZED SSPA & TWTA AMPLIFIERS

predistortion generator. Bremerson, et al, of Thomson-CSF demonstrated similar performance on a 13-watt 4 GHz TWTA using a Shottky barrier diode network in the linearizer.

7.5.3 Advantages and Disadvantages

The predistortion linearizer has several potential advantages for satellite operations. No closed loops are involved, so bandwidth is not constrained. The linearizer is separate from the PA, so the latter can be developed somewhat independently. The linearizer design is relatively simple, and it adds little mass and power to the spacecraft.

Key disadvantages of the predistortion linearizer is the extreme care required for alignment of phase and gain, and the need to individually marry each linearizer to its associated PA. Also, long-term stability of the PA and linearizer require evaluation to assure that long-term drifts do not degrade performance.

7.6 Cavity Feedback

To be effective, an RF feedback approach must

(1) be applied around several gain stages (30-40 dB open-loop amplifier gain) so that adequate gain remains in the closed-loop mode.

(2) band-limit the feedback path so that the loop gain falls below unity before the phase cross-over frequency is reached. (3) have small amplifier time delays in order to achieve usable bandwidths.

RF feedback is normally dismissed as a potential linearization technique for satellite transponders due to its inherent narrow-bandedness, par-

ticularly when TWT amplifiers are used. However, for the MSS application, with its relatively narrowband channels (1.4 MHz) and solid-state amplifiers with low time delay, RF feedback becomes an attractive linearization candidate.

7.6.1 Description of Operation

R. Place [1] has presented an RF feedback approach using a high-Q cavity resonator in the feedback path to limit the feedback bandwidth so that the loop gain falls below unity before the phase cross-over frequency is reached, assuring stable operation. Figure 7.6-1 shows an illustration of this approach. (In the figure, the cavity is shown in the output path. If it has excessive loss for this location, a low-loss directional coupler can be used at the amplifier output and the cavity located at the amplifier input or in the feedback path).

$$A = a\angle -\tau_a(\Delta f)\,(360°)$$

$$B = b\angle -\tau_b(\Delta f)\,(360°)$$

$$C = \frac{c}{\sqrt{1+\left(\frac{2\Delta f}{BW}\right)^2}}\angle -\tan^{-1}\left(\frac{2\Delta f}{BW}\right)$$

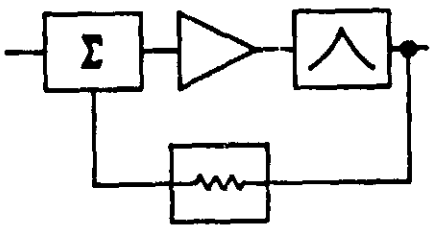

500271
KE550027/GAIL
1-15-85/MI

Figure 7.6-1 Cavity Feedback Implementation

The amplifier output in this configuration is given by

$$e_o = \frac{AC}{1+ABC}\,e_i + \frac{1}{1+ABC}\,e_{im}. \qquad (1)$$

The desired output is reduced by the factor C/(1+ABC) while the IM is reduced by the factor 1/(1+ABC). Thus, the IM improvement achieved is approximately equal to the gain reduction from the applied feedback.

Derivation of required cavity bandwidth

The required cavity bandwidth is determined by the amplifier time delay, T, and the amount of feedback applied. The bandwidth must be sufficiently narrow so that the open-loop gain falls below unity at the phase crossover frequency. The phase crossover frequency, f_c, is found by

$$\text{Phase} = 360(f_c)T + \tan^{-1}(f_c/BW) \qquad (2)$$

where $T = T_a + T_b$

= total time delay through the amplifier and feedback path

BW = resonator 3 dB bandwidth

Assuming a 45 degree phase margin, the allowable phase shift is 135 degrees.

Noting that the phase shift through the resonator must approach 90 degrees at the crossover frequency (since the resonator must provide significant attenuation at this frequency), eq (1) is then solved for the crossover frequency by

$$135 = 360(f_c)T + 90$$

$$f_c = T/8 \qquad (3)$$

The open loop gain must drop to unity or less at this frequency.
That is,

$$1 = ABC$$

$$= \frac{abc}{(1 + (f_c/BW)^2)^{1/2}}$$

By manipulating,

$$BW = \frac{2f_c}{((abc)^2-1)^{1/2}} \qquad (4)$$

Substituting eq(3) into eq(4), we obtain the required cavity bandwidth as

$$BW = \frac{1}{4T((abc)^2-1)^{1/2}} \qquad (5)$$

7.6.3 Performance

Eq (5) expresses the required cavity bandwidth as a function of the amplifier time delay and open-loop gain. Recalling that the IM reduction is also a function of open loop gain (in dB, IM improvement = 20 log (1+ABC), Place has plotted the required cavity bandwidth vs time delay and IM improvement. (See Figure 7.6-2).

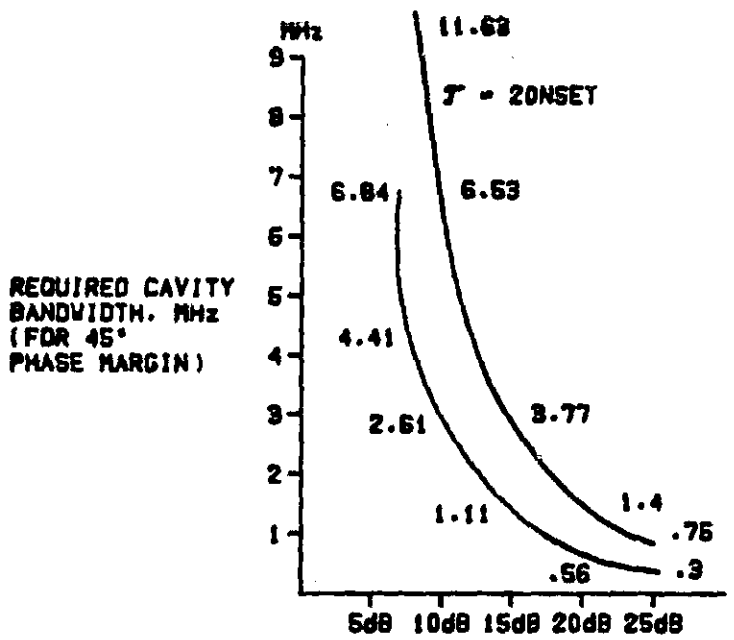

500272
KE650027/GAIL
1-18-84/MI

FIGURE 7.6-2 REQUIRED BANDWIDTH VS TIME DELAY AND C/I IMPROVEMENT

From Figure 7.6-2 it can be seen significant IM reduction can be achieved using a narrow cavity resonator in a negative feedback loop. For example, a 3-stage UHF amplifier may be expected to have a 40 dB gain with a time delay in the order of 20 ns or less. By using a 2.77 MHz bandwidth cavity resonator in a negative feedback configuration, approximately 15 dB IM improvement could be achieved across the 1.4 MHz MSS channel bandwidth. Greater improvements can be achieved with narrower bandwidths or less amplifier time delays. It should be noted that, if the bandwidth is narrowed too much more, it will begin to affect the channel passband response. Also, the amplifier gain will be correspondingly reduced as IM performance is improved, requiring additional gain stages ahead of the feedback loop.

7.6.4 Advantages and disadvantages

Advantages

Simple implementation The cavity feedback approach is straightforward and simple to implement. No critical phasing or matched detectors is required. Modern dielectric resonator technology enables achievement of the required narrow resonator bandwidth in a small volume and with extremely stable temperature performance. FACC has qualified and flown dielectric resonators with Qs greatly in excess of those required for this application.

Versatile. Unlike other approaches, eg, HELAPS, the feedback approach is relatively insensitive to dynamic range and type of modulation employed.

Unconditionally stable. The narrow-band resonator in the feedback loop provides unconditional stability.

Disadvantages.

Gain reduction. The amplifier gain is reduced by the IM improvement obtained, so 1-2 additional low-level gain stages must be added to make up this gain. This is a relatively minor impact.

Time delay control. In order to achieve effective usable bandwidth, time delays through the amplifier and feedback path must be controlled to be on the order of 20 ns or less. With broadband UHF solid-state amplifiers, this should not be a problem.

Mass. A moderate (< 1 kg) mass increase is required due to the additional dielectric resonator.